

## Manuscript Details

Manuscript number	COST_2018_821
Title	Vibration characteristics of a sandwich plate with viscoelastic periodic cores

### Abstract

The vibration characteristics of a sandwich plate with viscoelastic periodic cores are examined analytically and experimentally, which extends the previous research of corresponding periodic sandwich beam structure. Closed-form solutions for forced response and band structure of periodic sandwich plate are theoretically derived, providing computational support on the attenuation analysis. In the theoretical model, a new admissible displacement function for sandwich plate is proposed. Although it is used in free boundary condition in this paper, it is also suitable for clamped, simply supported, slipping, and elastic boundary conditions. The formation of the band gap is carefully studied, showing that the overall band gap is proved to be the intersection of all the cross-stream modal band gaps, which is quite different from a corresponding periodic beam structure. The parametric analysis shows further that the overall band gap could disappear when length ratio, element width, or core thickness exceeds a cut-off value, which provides a guidance in the band-gap design. The attenuation in a sandwich plate with viscoelastic periodic cores is mainly dominated by Bragg scattering mechanism in the band gap and by energy dissipation out of the band gap.

## **Submission Files Included in this PDF**

### **File Name [File Type]**

Manuscript.doc [Manuscript File]

Fig.8 BW.eps [Figure]

Fig.8 Color-vl.eps [Figure]

Fig.9 BW.eps [Figure]

Fig.9 Color.eps [Figure]

Fig.10 BW.eps [Figure]

Fig.10 Color.eps [Figure]

Fig.11 BW.eps [Figure]

Fig.11 Color.eps [Figure]

Fig.12 BW.eps [Figure]

Fig.12 Color.eps [Figure]

Fig.13 BW.eps [Figure]

Fig.13 Color.eps [Figure]

Fig.14 BW.eps [Figure]

Fig.14 Color.eps [Figure]

Fig.15 BW.eps [Figure]

Fig.15 Color.eps [Figure]

Fig.16(1).tif [Figure]

Fig.16(2).tif [Figure]

Fig.17.tif [Figure]

Fig.18.tif [Figure]

Fig.19 BW.eps [Figure]

Fig.19 Color.eps [Figure]

Fig.20.eps [Figure]

Fig.1.tif [Figure]

Fig.2.tif [Figure]

Fig.3.tif [Figure]

Fig.4.tif [Figure]

Fig.5.tif [Figure]

Fig.6.tif [Figure]

Fig.7 BW.eps [Figure]

Fig.7 Color.eps [Figure]

Table 1.doc [Table]

Table 2.doc [Table]

To view all the submission files, including those not included in the PDF, click on the manuscript title on your EVISE Homepage, then click 'Download zip file'.

1                   **Vibration characteristics of a sandwich plate with**  
2                   **viscoelastic periodic cores**

3

4                   Meiping Sheng<sup>\*a,b</sup>, Zhiwei Guo<sup>a,b</sup>, Qi Qin<sup>a,b</sup>, Yuanan He<sup>a</sup>

5

6                   <sup>a</sup>School of Marine Science and Technology, Northwestern Polytechnical University,

7                   127 Youyixilu, 710072 Xi'an, China

8                   <sup>b</sup>Research & Development Institute of Northwestern Polytechnical University in

9                   Shenzhen, 25 Gaoxin Nan Sidaogang, 518057 Shenzhen, China

10

11

12                  Number of Pages: 44

13                  Number of Figures: 20

14                  Number of Tables: 2

15

16

17

18

---

19                  \* Corresponding author: Meiping Sheng (phone: (+86) 029 8849 5861)

20                  E-mail addresses: Meiping Sheng (smp@nwpu.edu.cn), Zhiwei Guo (guozw891227@mail.nwpu.edu.cn),

21                  Qi Qin (34231@mail.nwpu.edu.cn), and Yuanan He (heyuanan@sina.com)

1    **ABSTRACT**

2       The vibration characteristics of a sandwich plate with viscoelastic periodic cores are  
3       examined analytically and experimentally, which extends the previous research of  
4       corresponding periodic sandwich beam structure. Closed-form solutions for forced  
5       response and band structure of periodic sandwich plate are theoretically derived,  
6       providing computational support on the attenuation analysis. In the theoretical model, a  
7       new admissible displacement function for sandwich plate is proposed. Although it is used  
8       in free boundary condition in this paper, it is also suitable for clamped, simply supported,  
9       slipping, and elastic boundary conditions. The formation of the band gap is carefully  
10      studied, showing that the overall band gap is proved to be the intersection of all the cross-  
11      stream modal band gaps, which is quite different from a corresponding periodic beam  
12      structure. The parametric analysis shows further that the overall band gap could disappear  
13      when length ratio, element width, or core thickness exceeds a cut-off value, which  
14      provides a guidance in the band-gap design. The attenuation in a sandwich plate with  
15      viscoelastic periodic cores is mainly dominated by Bragg scattering mechanism in the  
16      band gap and by energy dissipation out of the band gap. Owing to the combined effect of  
17      both mechanisms, the sandwich plate with viscoelastic periodic cores provides better  
18      attenuation performance than that with a uniform viscoelastic core. This research could  
19      possibly provide useful guidance for the researches and engineers on the design of plate-  
20      type damping structures.

21      *Keywords:* Band gap, Viscoelastic periodic cores, Sandwich plate, Vibration control.

22    **1. Introduction**

23       The sandwich structure has been studied and used for centuries and it plays a very  
24       important role in the engineering applications, including aircrafts [1], automobiles [2],

1 water-going vessels [3], architecture [4], etc. A sandwich structure is usually configured  
2 by two high-strength faces and a low-density core. With this configuration, the flexural  
3 rigidity and moment of inertia can be significantly increased in comparison to a  
4 homogeneous plate or a stiffened plate with the same mass. Thus, the sandwich structure  
5 provides a high stiffness-to-mass ratio, which is very important in the industrial design  
6 where reducing weight is a major concern.

7 Because of its great potential in applications, numerous researches have been  
8 conducted, including theoretical modeling methods [5-8], dynamic behaviors [9-11],  
9 structural configurations with various cores [12-18], industrial applications [1-4], and so  
10 on. Sandwich structures have been applied in different industrial fields for different  
11 purposes with corresponding different configurations. For example, a sandwich panel with  
12 a honeycomb core [18] is designed to obtain a high stiffness-to-mass ratio, which is  
13 particularly important in airplanes; and a heat-insulating core [19, 20] is used in a rocket  
14 or missile to protect internal structures or is used in the walls of buildings to maintain the  
15 temperature of room; while a porous core [15] is often used to isolate sound. The  
16 differences in these configurations mainly lie in the topology and material of the sandwich  
17 core.

18 Most sandwich structures have the advantage of reducing weight without losing  
19 stiffness. However, these lightweight sandwich panels may suffer from poor vibrational  
20 and acoustic performance, as a lightweight panel vibrates and radiates noise easily. In  
21 order to improve the vibro-acoustic characteristics, the sandwich structure with a  
22 viscoelastic core has been configured. As a viscoelastic core can provide great damping,  
23 the vibration of a sandwich structure can be significantly reduced by energy dissipation  
24 mechanism through great shearing deformation of the core. This traditional vibration-  
25 reduction technology is generally known as constrained-layer damping (CLD) treatment

1 [21-23], which has been widely applied in the engineering, including automobile panels,  
2 submarine hulls, and aircraft skins [24-26], owing to its simple structure and great  
3 potential in vibration control.

4 Generally, the CLD structure can provide outstanding attenuation in the higher  
5 frequency, which is quite acceptable for vibration control in the engineering. However, in  
6 the lower frequency, usually below several hundred hertz, the vibration-reduction  
7 performance of CLD structure is less acceptable as the long elastic wave is difficult to  
8 attenuate by damping. In order to improve the attenuation performance of CLD treatment,  
9 researchers have proposed various methods, including using electrorheological and  
10 magnetorheological cores [12, 16] and using active or smart surface panels [27, 28].  
11 These methods can improve the low-frequency attenuation performance of CLD treatment  
12 in some degree, however, the configurations could be quite complicated and expensive,  
13 which limits their applications in the practical engineering. Therefore, a simple and new  
14 damping structure to further improve the CLD treatment is still in great need.

15 In the last two decades, phononic crystals [29-31] and metamaterials [32-34] have  
16 triggered heated discussion for their potential in vibration and noise control. In essence,  
17 phononic crystals and metamaterials are often composed of periodic artificial elements  
18 alternated in one, two, and three dimensions. Because of the spatial periodicity, waves in  
19 the band gaps cannot propagate without attenuation and waves in the pass bands can  
20 propagate freely, which is called wave-filtering behavior. As no wave propagates in the  
21 band gaps, the vibration in the band gaps will be reduced. Thus, the periodic structure has  
22 gradually become a new approach to reduce noise and vibration. Due to the great potential  
23 in vibration control for periodic structures, the sandwich beam with periodic cores has  
24 been studied by several researchers with the focus on various aspects. Ruzzene et al. [35]  
25 and Wen et al. [36] studied the effect of negative Poisson's ratio in the periodic auxetic

cores on the band-gap properties. Following their researches, Badran et al. [37] further studied the vibration characteristics of a sandwich beam with elastic periodic cores by finite element method (FEM). In his study, the hard core was designed with its Young's modulus larger than that of the face layer in order to obtain a broad band-gap width. In addition, Chen et al. [38] also studied the sandwich beam with periodic assemblies, with the specific focus on the effect of moving load and elastic foundation on the wave-propagation characteristics. Each of these studies provides a specific view to understand the physical insight of the periodic sandwich beam. However, in the above researches, the periodic cores are only considered as purely elastic materials, while the damping of cores is neglected. In fact, the core of a sandwich structure usually possesses relative greater damping than the face sheets. It has been proved that damping also has a great effect on the band-gap performance in phononic crystals and metamaterials [39-42], which helps to improve the attenuation performance of a periodic structure. Considering this, the authors studied the flexural wave attenuation in a sandwich beam with viscoelastic periodic cores in the previous research [43], where the damping of periodic cores are include in the model. In fact, this structure can be considered as a new damping structure, which is called in Reference [43] as periodic constrained-layer damping (PCLD) treatment. Owing to the combined attenuation mechanisms of both Bragg scattering effect arising from structural periodicity and energy dissipation effect arising from damping, a sandwich beam with PCLD treatment can effectively reduce vibrations of much lower frequencies than that with traditional CLD treatment.

In the previous research for the sandwich structure with viscoelastic periodic cores, the structure is limited to a one-dimensional sandwich beam, where only plane wave along cross-stream direction is considered. However, in the practical engineering, most sandwich structures have two dimensions with plate-type configurations instead of beam-

1 type configurations, and thus both plane wave and non-plane wave along cross-stream  
2 direction exist in the structure. This phenomenon results that the band-gap characteristicis  
3 of a one-dimensional sandwich beam with viscoelastic periodic cores cannot represent the  
4 characteristcis of a two-dimensional sandwich plate with viscoelastic periodic cores.  
5 When the one-dimensional periodic sandwich structure is extended to two dimensions,  
6 some new physical phenomenon can be found and need to be physically explained. For  
7 example, the band-gap width of a periodic sandwich plate could be much smaller than that  
8 of a corresponding periodic sandwich beam, and even that the band gap of the plate  
9 structure could disappear when some parameters exceed a cut-off value, which never  
10 happens in the corrsponding beam structure. There are also some other important physical  
11 insights in the sandwich plate with viscoelastic periodic cores, which needs further  
12 research.

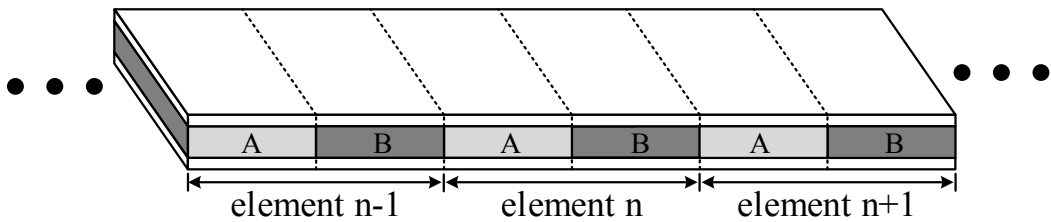
13 From the above, it can be seen that extending the research of a sandwich beam with  
14 viscoelastic periodic cores to the research of a sandwich plate with viscoelastic periodic  
15 cores has necessary practical meaning and important physical meaning. Therefore, in this  
16 paper, the vibration characteristics of a sandwich plate with viscoelastic periodic cores are  
17 examined analytically and experimentally, which extends the previous research of  
18 corresponding periodic sandwich beam structure. The forced response and band structure  
19 of the periodic sandwich plate are theoretically derived, which provides analytical support  
20 on the analysis of vibration characteristics. The band-gap formation mechanism for the  
21 periodic sandwich plate is thoroughly studied and the combined attenuation performance  
22 resulted by both Bragg scattering and energy dissipation is also examined, providing proof  
23 that the plate with PCLD treatment has superior attenuation performance than that with  
24 CLD treatment. Finally, an experiment is designed and conducted to prove the practical  
25 attenuation performance of the sandwich plate with viscoelastic periodic cores and also to

1 verify the theoretical model established in this paper.

## 2 Configuration and formulation

### 2.1 Configuration of periodic sandwich plate and dynamic assumptions

4 The periodic sandwich plate considered in this paper is composed of two elastic  
 5 uniform surface layers and repeated viscoelastic periodic cores, as shown in **Fig. 1**. Each  
 6 element of the periodic sandwich plate can be considered as two sub sandwich plates  
 7 joining together end to end, of which the cores are labelled as core A and core B. This  
 8 plate-type structure is extended from a sandwich beam with viscoelastic periodic cores  
 9 [43] and shows more complicated attenuation performance for flexural wave due to its  
 10 limited dimension along width direction.

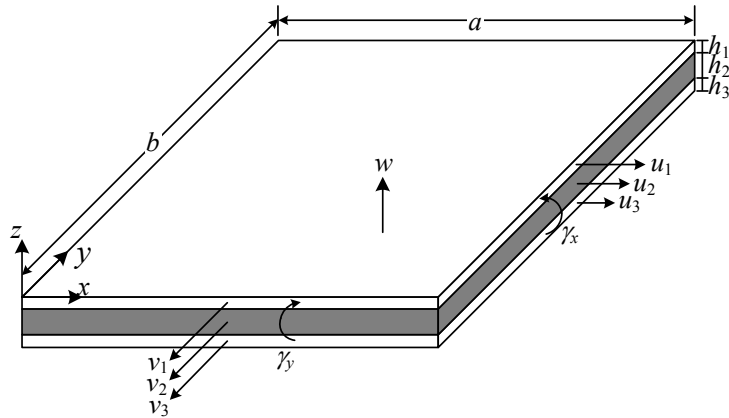


12 **Fig. 1** Schematic diagram of an infinite sandwich plate with viscoelastic periodic cores.

13 In order to establish the theoretical model for solving the vibrational problem of  
 14 periodic sandwich plate, the theoretical derivation is based on the following assumptions.  
 15 The two surface layers are made of linear elastic materials, while the two periodically  
 16 repeated cores are made of linear viscoelastic materials with complex Young's moduli  
 17 and complex shear moduli. The in-plane displacements of all the three layers are  
 18 considered, while slipping is not permitted between each two neighboring layers. As the  
 19 shear moduli of sandwich cores are usually far smaller than those of surface layers, the  
 20 shearing effect is only considered in the cores, thus the sandwich cores only have shearing  
 21 deformation without normal deformation. Furthermore, at the same in-plane location ( $x, y$ ),  
 22 the transverse displacements in all the three layers keep identical.

1    **2.2 Dynamic equations of a sandwich plate with a monolithic core**

2       The schematic diagram of a sandwich plate with a monolithic core is Shown in **Fig. 2**.  
 3       The dynamic equations of such a homogeneous structure are briefly discussed in this  
 4       subsection to provide basic theory for the vibrational modelling in the finite or infinite  
 5       periodic sandwich plate.



7       **Fig. 2.** Coordinates and notations of a sandwich plate.

8       The material properties of each layer in the sandwich plate shown in **Fig. 2** are  
 9       specified as Young's modulus  $E_i$ , shear modulus  $G_i$ , density  $\rho_i$ , and Poisson's ratio  
 10       $\nu_i$  ( $i=1, 2, 3$ ). The length, width, and thickness of the sandwich plate are labelled as  $a$ ,  
 11       $b$ , and  $h_i$ , respectively. The transverse and in-plane displacements of each layer are  
 12      specified respectively as  $w$ ,  $u_i$ , and  $v_i$ , and the local rotation displacements of the  
 13      viscoelastic core are denoted as  $\gamma_x$  and  $\gamma_y$ . The viscosity of the sandwich core is  
 14      considered by using a complex Young's modulus  $E_2 = E_{2s} [1 + j\eta(\omega)]$ , where  $E_{2s}$  is  
 15      storage modulus for a purely elastic material and  $\eta(\omega)$  is generally known as material  
 16      loss factor. In fact, there are also other methods to represent the viscosity of a viscoelastic  
 17      material, such as using the concept of viscosity coefficient used by Moiseyenko et al. [40],  
 18      Wang et al. [42], and Guo et al. [43]. In this paper, the material viscosity is represented by

1 material loss factor for convenient purpose, as the material loss factor of a viscoelastic  
 2 material can be directly tested in the damping experiment.

3 The strain energy  $E_{\text{pot}}^i$  and kinematic energy  $E_{\text{kin}}^i$  of the two surface layers can be  
 4 expressed respectively as

$$5 \quad E_{\text{pot}}^i = \frac{1}{2} B_i \int \int \left[ u_{ix}^2 + 2\nu_i u_{ix} v_{iy} + v_{iy}^2 + \nu_{ia} (u_{iy} + v_{ix})^2 \right] dx dy \quad (i=1,3) \\ + \frac{1}{2} D_i \int \int \left[ w_{xx}^2 + 2\nu_i w_{xx} w_{yy} + w_{yy}^2 + 2(1-\nu_i) w_{xy}^2 \right] dx dy$$

6 and

$$7 \quad E_{\text{kin}}^i = \frac{1}{2} \int \int \left[ m_i (\ddot{u}_i^2 + \dot{v}_i^2 + \dot{w}^2) + J_i (\dot{w}_x^2 + \dot{w}_y^2) \right] dx dy \quad (i=1,3). \quad (2)$$

8 The strain energy  $E_{\text{pot}}^2$  and kinematic energy  $E_{\text{kin}}^2$  of the sandwich core can be  
 9 expressed respectively as

$$10 \quad E_{\text{pot}}^2 = \frac{1}{2} G_h \int \int (\gamma_x^2 + \gamma_y^2) dx dy \quad (3)$$

11 and

$$12 \quad E_{\text{kin}}^2 = \frac{1}{2} \int \int \left[ m_2 (\ddot{u}_2^2 + \dot{v}_2^2 + \dot{w}^2) + J_2 (\dot{\theta}_2^2 + \dot{\phi}_2^2) \right] dx dy. \quad (4)$$

13 In Eqs. (1) – (4), the dots above variables denote partial differentiation with respect  
 14 to time variable  $t$ ,  $B_i = E_i h_i / (1 - \nu_i^2)$ ,  $D_i = E_i h_i^3 / 12 (1 - \nu_i^2)$ ,  $\nu_{ia} = (1 - \nu_i) / 2$ ,  $G_h = G_2 / h_2$ ,

15  $\gamma_x = (u_3 - u_1 - d w_x) / h_2$ ,  $\gamma_y = (v_3 - v_1 - d w_y) / h_2$ ,  $d = h_2 + (h_1 + h_3) / 2$ ,  $m_i = \rho_i h_i$ ,

16  $J_i = \rho_i h_i^3 / 12$ ,  $\theta_2 = [u_1 - u_3 - (h_1 + h_3) w_x / 2] / h_2$ , and  $\varphi_2 = [v_1 - v_3 - (h_1 + h_3) w_y / 2] / h_2$ .

17 The total strain energy and total kinematic energy can then be expressed as

18  $E_{\text{kin}} = \sum_{i=1}^3 E_{\text{kin}}^i$  and  $E_{\text{pot}} = \sum_{i=1}^3 E_{\text{pot}}^i$ , respectively. By using Hamilton's principle

19  $\delta \int_{t_0}^{t_1} (E_{\text{kin}} - E_{\text{pot}}) dt = 0$  and considering harmonic oscillation assumptions  $u_1 = U_1 e^{j\omega t}$ ,

20  $v_1 = V_1 e^{j\omega t}$ ,  $u_3 = U_3 e^{j\omega t}$ ,  $V_3 = V_3 e^{j\omega t}$ , and  $w = W e^{j\omega t}$ , the equations of motion for a

1 homogeneous sandwich plate can be obtained as

$$2 \quad \begin{bmatrix} L_{11} & L_{12} & L_{13} & L_{14} & L_{15} \\ L_{21} & L_{22} & L_{23} & L_{24} & L_{25} \\ L_{31} & L_{32} & L_{33} & L_{34} & L_{35} \\ L_{41} & L_{42} & L_{43} & L_{44} & L_{45} \\ L_{51} & L_{52} & L_{53} & L_{54} & L_{55} \end{bmatrix} \begin{pmatrix} u_1 \\ v_1 \\ u_3 \\ v_3 \\ w \end{pmatrix} = \begin{pmatrix} 0 \\ 0 \\ 0 \\ 0 \\ f_z \end{pmatrix}, \quad (5)$$

3 where  $L_{ij}$  ( $i, j = 1, \dots, 5$ ) are differential operators with respect to space variables  $x$  and  
4  $y$ , which are defined in Eqs. (A.32) – (A.45) in Appendix A.

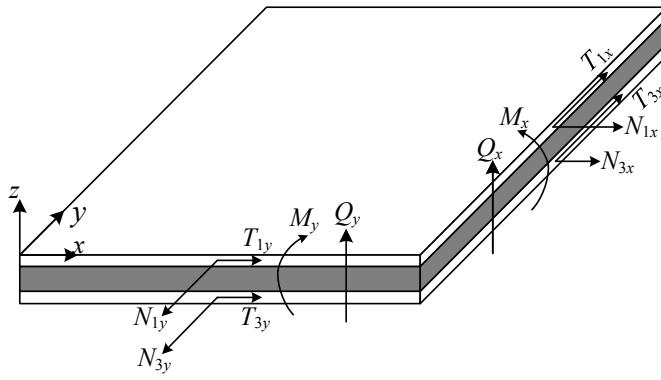


Fig. 3. Denotations of generalized forces in a sandwich plate.

7 According to Hamilton's principle, the generalized forces (see Fig. 3) at the cross  
8 sections of  $x = 0, a$  and  $y = 0, b$  can be expressed respectively as

$$9 \quad \begin{cases} N_{1x} = B_1(u_{1x} + \nu_1 v_{1y}), T_{1x} = \nu_{1a} B_1(v_{1x} + u_{1y}), N_{3x} = B_3(u_{3x} + \nu_3 v_{3y}), T_{3x} = \nu_{3a} B_3(v_{3x} + u_{3y}) \\ Q_x = -(D_1 + D_3)w_{xxx} - [D_1(2 - \nu_1) + D_3(2 - \nu_3)]w_{xyy} + (-G_h du_1 + G_h du_3 + d^2 G_h w_x) \\ M_x = (D_1 + D_3)w_{xx} + (D_1 \nu_1 + D_3 \nu_3)w_{yy} \end{cases} \quad (6)$$

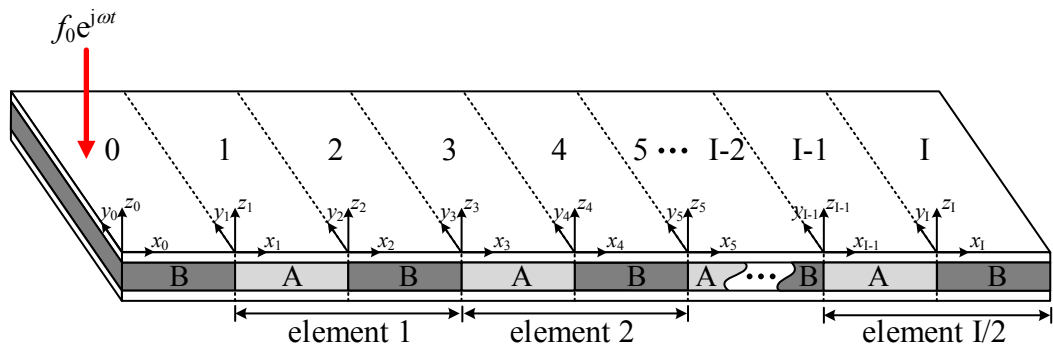
10 and

$$11 \quad \begin{cases} N_{1y} = B_1(v_{1y} + \nu_1 u_{1x}), T_{1y} = \nu_{1a} B_1(u_{1y} + v_{1x}), N_{3y} = B_3(v_{3y} + \nu_3 u_{3x}), T_{3y} = \nu_{3a} B_3(u_{3y} + v_{3x}) \\ Q_y = -(D_1 + D_3)w_{yyy} - [D_1(2 - \nu_1) + D_3(2 - \nu_3)]w_{xxy} + (-G_h dv_1 + G_h dv_3 + d^2 G_h w_y) \\ M_y = (D_1 + D_3)w_{yy} + (D_1 \nu_1 + D_3 \nu_3)w_{xx} \end{cases}, \quad (7)$$

12 where  $N_{1x}$ ,  $N_{3x}$ ,  $N_{1y}$ , and  $N_{3y}$  are axial forces;  $T_{1x}$ ,  $T_{3x}$ ,  $T_{1y}$ , and  $T_{3y}$  are tangential  
13 forces;  $M_x$  and  $M_y$  are bending moments; and  $Q_x$  and  $Q_y$  are shearing forces.

1    **2.3 Forced response of a finite periodic sandwich plate**

2       Shown in **Fig. 4** is a finite periodic sandwich plate, which is composed of  $I+1$  sub  
 3       sandwich plates with core A or core B, labelled from 0 to I. The harmonic excitation  
 4        $f_0 e^{j\omega t}$  is applied at sub sandwich plate 0 and the vibration response of each sub sandwich  
 5       plate can be determined by the following theoretical derivation. Then the transmission  
 6       characteristics of the periodic sandwich plate can be further examined.



7       **Fig. 4.** A finite periodic sandwich plate.

8       In order to obtain the vibration response of a finite periodic sandwich plate in this  
 9       subsection and to obtain the band structure of an infinite periodic sandwich plate in the  
 10      next subsection, the admissible function of displacements for each sub sandwich plate  
 11      must be known. However, in the available literature, the appropriate admissible function  
 12      has not been found to satisfy the calculation of both forced response and band structure in  
 13      the periodic sandwich plate. In order to solve this problem, a new admissible displacement  
 14      function of a sandwich plate is proposed in this paper by extending the admissible  
 15      displacement function used in a single-layer thin plate proposed by Li et al. [44], where  
 16      the admissible function is composed of a main component to make contribution to the  
 17      displacement and a supplementary component introduced to take care of possible  
 18      discontinuities of derivatives at the edges of plate.

20      The proposed admissible function for the in-plane displacements  $u_{1i}$ ,  $v_{1i}$ ,  $u_{3i}$ , and

1  $v_{3i}$  and the transverse displacement  $w_i$  of the  $i^{\text{th}}$  sub sandwich plate can be expressed as

$$2 \quad \begin{cases} u_{1i}(x_i, y_i) = \sum_{m=0}^{\infty} \sum_{n=0}^{\infty} U_{1imn} \cos \lambda_{im} x_i \cos \lambda_{in} y_i + \sum_{l=1}^2 \left[ \zeta_{ib}^l(y_i) \sum_{m=0}^{\infty} c_{1ium}^l \cos \lambda_{im} x_i + \zeta_{ia}^l(x_i) \sum_{n=0}^{\infty} d_{1iun}^l \cos \lambda_{in} y_i \right] \\ v_{1i}(x_i, y_i) = \sum_{m=0}^{\infty} \sum_{n=0}^{\infty} V_{1imn} \cos \lambda_{im} x_i \cos \lambda_{in} y_i + \sum_{l=1}^2 \left[ \zeta_{ib}^l(y_i) \sum_{m=0}^{\infty} c_{1ivm}^l \cos \lambda_{im} x_i + \zeta_{ia}^l(x_i) \sum_{n=0}^{\infty} d_{1ivn}^l \cos \lambda_{in} y_i \right] \\ u_{3i}(x_i, y_i) = \sum_{m=0}^{\infty} \sum_{n=0}^{\infty} U_{3imn} \cos \lambda_{im} x_i \cos \lambda_{in} y_i + \sum_{l=1}^2 \left[ \zeta_{ib}^l(y_i) \sum_{m=0}^{\infty} c_{3ium}^l \cos \lambda_{im} x_i + \zeta_{ia}^l(x_i) \sum_{n=0}^{\infty} d_{3iun}^l \cos \lambda_{in} y_i \right], \\ v_{3i}(x_i, y_i) = \sum_{m=0}^{\infty} \sum_{n=0}^{\infty} V_{3imn} \cos \lambda_{im} x_i \cos \lambda_{in} y_i + \sum_{l=1}^2 \left[ \zeta_{ib}^l(y_i) \sum_{m=0}^{\infty} c_{3ivm}^l \cos \lambda_{im} x_i + \zeta_{ia}^l(x_i) \sum_{n=0}^{\infty} d_{3ivn}^l \cos \lambda_{in} y_i \right] \\ w_i(x_i, y_i) = \sum_{m=0}^{\infty} \sum_{n=0}^{\infty} W_{imn} \cos \lambda_{im} x_i \cos \lambda_{in} y_i + \sum_{l=1}^4 \left[ \zeta_{ib}^l(y_i) \sum_{m=0}^{\infty} c_{iwm}^l \cos \lambda_{im} x_i + \zeta_{ia}^l(x_i) \sum_{n=0}^{\infty} d_{iwn}^l \cos \lambda_{in} y_i \right] \end{cases}, \quad (8)$$

3 where  $\lambda_{im} = m\pi/a_i$  and  $\lambda_{in} = n\pi/b_i$ . The terms  $U_{1imn}$ ,  $V_{1imn}$ ,  $U_{3imn}$ ,  $V_{3imn}$ ,  $W_{imn}$ ,  $c_{1ium}^l$ ,

4  $d_{1iun}^l$ ,  $c_{1ivm}^l$ ,  $d_{1ivn}^l$ ,  $c_{3ium}^l$ ,  $d_{3iun}^l$ ,  $c_{3ivm}^l$ ,  $d_{3ivn}^l$ ,  $c_{iwm}^l$ , and  $d_{iwn}^l$  represent unknown expansion

5 coefficients, which need to be determined by both boundary equations and governing

6 differential equations. The admissible displacement function proposed in Eq. (8) are used

7 to satisfy free, continuous, and periodic boundary conditions involved in this paper. Apart

8 from these boundary conditions, it can also be used in other boundary conditions,

9 including but not limited to clamped, simply supported, slipping, and elastic boundary

10 conditions. In Eq. (8), the terms  $\zeta_{ia}^l(x_i)$ ,  $\zeta_{ib}^l(y_i)$ ,  $\zeta_{ia}^l(x_i)$ , and  $\zeta_{ib}^l(y_i)$  are chosen in the

11 form of trigonometric functions and are defined as

$$12 \quad \begin{aligned} \xi_{is}(\chi_i) &= \begin{bmatrix} \xi_{is}^1(\chi_i) & \xi_{is}^2(\chi_i) & \xi_{is}^3(\chi_i) & \xi_{is}^4(\chi_i) \end{bmatrix}^T \\ &= \begin{bmatrix} \sin\left(\frac{\pi\chi_i}{2s_i}\right) & \cos\left(\frac{\pi\chi_i}{2s_i}\right) & \sin\left(\frac{3\pi\chi_i}{2s_i}\right) & \cos\left(\frac{3\pi\chi_i}{2s_i}\right) \end{bmatrix}^T \end{aligned} \quad (9)$$

13 and

$$14 \quad \zeta_{is}(\chi_i) = \mathbf{A} \xi_{is}(\chi_i), \quad (10)$$

15 where variable  $\chi_i$  represents  $x_i$  or  $y_i$  and the subscript  $s$  in the above equation

16 represents correspondingly  $a$  or  $b$ . The term  $\mathbf{A}$  is a  $2 \times 4$  matrix and is written as

$$1 \quad \mathbf{A} = \begin{bmatrix} 1 & 0 & 0 & 0 \\ 0 & 1 & 0 & 0 \end{bmatrix}.$$

2        The derivatives of the trigonometric function vector  $\xi_{is}(\chi_i)$  with respect to  $\chi_i$  can  
 3        be expressed by  $\xi_{is}(\chi_i)$  itself. The first- to fourth-order derivatives used in the boundary  
 4        equations and governing differential equations can be determined as

$$5 \quad \begin{cases} \xi_{is}^{(1)}(\chi_i) = \mathbf{B}_{is1} \mathbf{B}_{is0} \xi_{is}(\chi_i), & \xi_{is}^{(2)}(\chi_i) = \mathbf{B}_{is2} \xi_{is}(\chi_i) \\ \xi_{is}^{(3)}(\chi_i) = \mathbf{B}_{is3} \mathbf{B}_{is0} \xi_{is}(\chi_i), & \xi_{is}^{(4)}(\chi_i) = \mathbf{B}_{is4} \xi_{is}(\chi_i) \end{cases}, \quad (11)$$

6        where matrices  $\mathbf{B}_{is0}$  to  $\mathbf{B}_{is4}$  are defined in Eqs. (A.46) – (A.50) in Appendix A.

7        In order to make it possible for separation of variable in the governing equations,  
 8         $\xi_{is}(\chi_i)$  is expanded in the form of cosine series as

$$9 \quad \xi_{is}(\chi_i) = \sum_{r=0}^{\infty} \tau_r \cos \lambda_{isr} \chi_i, \quad (12)$$

10        where  $\tau_r$  is defined in Eq. (A.51) in Appendix A. With Eqs. (11) and (12), the first- to  
 11        fourth-order derivatives of  $\xi_{is}(\chi_i)$  can all be expressed in the form of cosine series

$$12 \quad \begin{cases} \xi_{is}^{(1)}(\chi_i) = \sum_{r=0}^{\infty} \mathbf{a}_{is1r} \cos \lambda_{isr} \chi_i, & \xi_{is}^{(2)}(\chi_i) = \sum_{r=0}^{\infty} \mathbf{a}_{is2r} \cos \lambda_{isr} \chi_i \\ \xi_{is}^{(3)}(\chi_i) = \sum_{r=0}^{\infty} \mathbf{a}_{is3r} \cos \lambda_{isr} \chi_i, & \xi_{is}^{(4)}(\chi_i) = \sum_{r=0}^{\infty} \mathbf{a}_{is4r} \cos \lambda_{isr} \chi_i \end{cases}, \quad (13)$$

13        where  $\mathbf{a}_{isjr} = [\alpha_{isjr}^1 \quad \alpha_{isjr}^2 \quad \alpha_{isjr}^3 \quad \alpha_{isjr}^4]^T$  ( $s = a, b; j = 1, 2, 3, 4$ ) is a  $4 \times 1$  column vector  
 14        and is given as  $\mathbf{a}_{is1r} = \mathbf{B}_{is1} \mathbf{B}_{is0} \mathbf{a}_{is0r}$ ,  $\mathbf{a}_{is2r} = \mathbf{B}_{is2} \mathbf{a}_{is0r}$ ,  $\mathbf{a}_{is3r} = \mathbf{B}_{is3} \mathbf{B}_{is0} \mathbf{a}_{is0r}$ ,  $\mathbf{a}_{is4r} = \mathbf{B}_{is4} \mathbf{a}_{is0r}$ ,  
 15        in which  $\mathbf{a}_{is0r} = \tau_r$ .

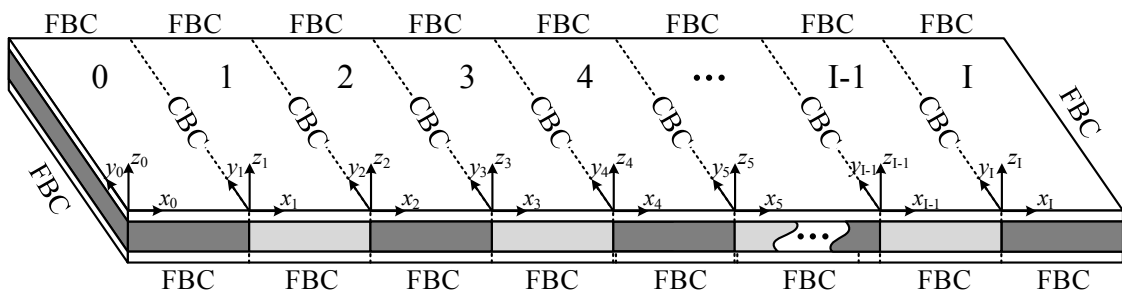
16        From Eqs. (10) – (13), the first- to fourth-order derivatives of  $\zeta_{is}(\chi_i)$  can be further  
 17        expressed as

$$18 \quad \zeta_{is}^{(j)}(\chi_i) = \sum_{r=0}^{\infty} \beta_{isjr} \cos \lambda_{isr} \chi_i \quad (j = 1, 2, 3, 4), \quad (14)$$

1 where  $\beta_{isjr} = \mathbf{A}\alpha_{isjr}$ .

2 The above theoretical statements present the basic theory about the admissible  
 3 displacement function of a sandwich plate. In the following, the characteristic equations  
 4 of the forced response in a finite periodic sandwich plate is determined by considering  
 5 both boundary equations and governing equations.

6 Shown in **Fig. 5** is a finite periodic sandwich plate with free boundary conditions  
 7 (FBCs) at plate edges and continuous boundary conditions (CBCs) between each two  
 8 neighboring sub sandwich plates. The boundary equations can be classified in three types  
 9 as shown in the following.



11 **Fig. 5.** Boundary conditions in a finite periodic sandwich plate.

12 (1) FBCs along  $x$  direction

13 Each sub sandwich plate (labelled from 0 to I) is in free boundary condition at  
 14  $y_i = 0$  and  $y_i = b_i$ , thus the generalized forces should be zero, which can be written as

$$15 (y_i = 0): \begin{cases} N_{1iy}(x_i, 0) = 0 \\ T_{1iy}(x_i, 0) = 0 \\ N_{3iy}(x_i, 0) = 0 \\ T_{3iy}(x_i, 0) = 0 \\ Q_{iy}(x_i, 0) = 0 \\ M_{iy}(x_i, 0) = 0 \end{cases} (y_i = b_i): \begin{cases} N_{1iy}(x_i, b_i) = 0 \\ T_{1iy}(x_i, b_i) = 0 \\ N_{3iy}(x_i, b_i) = 0 \\ T_{3iy}(x_i, b_i) = 0 \\ Q_{iy}(x_i, b_i) = 0 \\ M_{iy}(x_i, b_i) = 0 \end{cases} \quad (15)$$

16 (2) FBCs at the left and right end of the whole structure

17 As FBCs are assumed at both ends of the periodic sandwich plate ( $x_0 = 0$  and

1       $x_1 = a_1$ ), the corresponding generalized forces must be zero, namely

$$2 \quad (x_0 = 0): \begin{cases} N_{10x}(0, y_i) = 0 \\ T_{10x}(0, y_i) = 0 \\ N_{30x}(0, y_i) = 0 \\ T_{30x}(0, y_i) = 0 \\ Q_{0x}(0, y_i) = 0 \\ M_{0x}(0, y_i) = 0 \end{cases} \quad (x_1 = a_1): \begin{cases} N_{1Ix}(a_1, y_i) = 0 \\ T_{1Ix}(a_1, y_i) = 0 \\ N_{3Ix}(a_1, y_i) = 0 \\ T_{3Ix}(a_1, y_i) = 0 \\ Q_{Ix}(a_1, y_i) = 0 \\ M_{Ix}(a_1, y_i) = 0 \end{cases} \quad (16)$$

3      (3) CBCs between each two neighboring sub sandwich plates

4      At the interface between sub sandwich plate  $i-1$  and sub sandwich plate  $i$  (

5       $x_{i-1} = a_{i-1}$  or  $x_i = 0$  for  $1 \leq i \leq I$  ), the generalized displacements must be continuous and

6      the generalized forces must satisfy the equilibrium condition, namely

$$7 \quad \begin{cases} u_{l(i-1)}(a_{i-1}, y_{i-1}) = u_{li}(0, y_i) \\ v_{l(i-1)}(a_{i-1}, y_{i-1}) = v_{li}(0, y_i) \\ u_{3(i-1)}(a_{i-1}, y_{i-1}) = u_{3i}(0, y_i) \\ v_{3(i-1)}(a_{i-1}, y_{i-1}) = v_{3i}(0, y_i) \\ w_{(i-1)}(a_{i-1}, y_{i-1}) = w_i(0, y_i) \\ \theta_{(i-1)}(a_{i-1}, y_{i-1}) = \theta_i(0, y_i) \end{cases} \quad \begin{cases} N_{l(i-1)x}(a_{i-1}, y_{i-1}) = N_{lx}(0, y_i) \\ T_{l(i-1)x}(a_{i-1}, y_{i-1}) = T_{lx}(0, y_i) \\ N_{3(i-1)x}(a_{i-1}, y_{i-1}) = N_{3x}(0, y_i) \\ T_{3(i-1)x}(a_{i-1}, y_{i-1}) = T_{3x}(0, y_i) \\ Q_{(i-1)x}(a_{i-1}, y_{i-1}) = Q_{x}(0, y_i) \\ M_{(i-1)x}(a_{i-1}, y_{i-1}) = M_{x}(0, y_i) \end{cases} \quad (17)$$

8      In the following calculation, the infinite series in Eq. (8) are truncated to  $m = M$   
 9      and  $n = N$ , and those in Eqs. (12) – (14) are truncated to  $r = M$  or  $r = N$ . By taking  
 10     the advantage of Eqs. (6) – (14), the 36 boundary expressions shown in Eqs. (15) – (17)  
 11     can be rewritten in a matrix form as

$$12 \quad \mathbf{H}\mathbf{p} = \mathbf{Q}\mathbf{a}, \quad (18)$$

13     where  $\mathbf{p} = [\mathbf{p}_0, \mathbf{p}_1, \dots, \mathbf{p}_I]^T$  and  $\mathbf{a} = [\mathbf{a}_0, \mathbf{a}_1, \dots, \mathbf{a}_I]^T$ . The term  $\mathbf{p}_i$  and  $\mathbf{a}_i$  are defined as

14      $\mathbf{p}_i = [\mathbf{c}_{liu} \ \mathbf{d}_{liu} \ \mathbf{c}_{liv} \ \mathbf{d}_{liv} \ \mathbf{c}_{3iu} \ \mathbf{d}_{3iu} \ \mathbf{c}_{3iv} \ \mathbf{d}_{3iv} \ \mathbf{c}_{iw} \ \mathbf{d}_{iw}]^T$  and  $\mathbf{a}_i = [\mathbf{U}_{li} \ \mathbf{V}_{li} \ \mathbf{U}_{3i} \ \mathbf{V}_{3i} \ \mathbf{W}_i]^T$ , respectively.

15     The vector  $\mathbf{c}_{liu}$  in the expression of  $\mathbf{p}_i$  is given as  $\mathbf{c}_{liu} = [c_{liu0}^1, c_{liu1}^1, \dots, c_{liuM}^1, c_{liu0}^2, \dots,$   
 16      $c_{liuM}^2]$  and  $\mathbf{d}_{liu}$  is given as  $\mathbf{d}_{liu} = [d_{liu0}^1, d_{liu1}^1, \dots, d_{liuN}^1, d_{liu0}^2, \dots, d_{liuN}^2]$ . The elements of

1 vectors ( $\mathbf{c}_{1iv}$ ,  $\mathbf{c}_{3iu}$ ,  $\mathbf{c}_{3iv}$ , and  $\mathbf{c}_{iw}$ ) and vectors ( $\mathbf{d}_{1iv}$ ,  $\mathbf{d}_{3iu}$ ,  $\mathbf{d}_{3iv}$ , and  $\mathbf{d}_{iw}$ ) present  
 2 respectively similar arrangements as those of  $\mathbf{c}_{1iu}$  and  $\mathbf{d}_{1iu}$ , except that  $\mathbf{c}_{iw}$  has  
 3  $4 \times (M+1)$  elements and  $\mathbf{d}_{iw}$  has  $4 \times (N+1)$  elements. The vector  $\mathbf{U}_{1i}$  in the  
 4 expression of  $\mathbf{a}_i$  can be written as  $\mathbf{U}_{1i} = [U_{1i00}, U_{1i01}, \dots, U_{1i0N}, U_{1i10}, U_{1i11}, \dots, U_{1i1N}, \dots,$   
 5  $U_{1imn}, \dots, U_{1iM0}, U_{1iM1}, \dots, U_{1iMN}]$ . The elements of vectors  $\mathbf{V}_{1i}$ ,  $\mathbf{U}_{3i}$ ,  $\mathbf{V}_{3i}$ , and  $\mathbf{W}_{1i}$   
 6 present similar arrangement as those of  $\mathbf{U}_{1i}$ .

7 From Eq. (18), vector  $\mathbf{p}$  can be expressed by vector  $\mathbf{a}$ , namely

$$8 \quad \mathbf{p} = \mathbf{H}^{-1} \mathbf{Q} \mathbf{a}. \quad (19)$$

9 From boundary constraints, a set of  $12 \times (M+N+2) \times (I+1)$  equations can be  
 10 obtained in Eq. (18) against a total of  $12 \times (M+N+2) \times (I+1) + 5 \times (M+1) \times (N+1) \times (I+1)$   
 11 unknown expansion coefficients. Thus additional  $5 \times (M+1) \times (N+1) \times (I+1)$  governing  
 12 differential equations need to be provided to finally determine the overall unknown  
 13 coefficients.

14 Assuming that a harmonic point force  $F_{i0} e^{j\omega t}$  is applied at position  $(x_{i0}, y_{i0})$  on  
 15 the  $i^{\text{th}}$  sub sandwich plate, from Eq. (5), the governing differential equation of the  $i^{\text{th}}$  sub  
 16 sandwich plate can be expressed as

$$17 \quad \begin{bmatrix} L_{11} & L_{12} & L_{13} & L_{14} & L_{15} \\ L_{21} & L_{22} & L_{23} & L_{24} & L_{25} \\ L_{31} & L_{32} & L_{33} & L_{34} & L_{35} \\ L_{41} & L_{42} & L_{43} & L_{44} & L_{45} \\ L_{51} & L_{52} & L_{53} & L_{54} & L_{55} \end{bmatrix} \begin{pmatrix} u_{1i} \\ v_{1i} \\ u_{3i} \\ v_{3i} \\ w_i \end{pmatrix} = \begin{pmatrix} 0 \\ 0 \\ 0 \\ 0 \\ F_{i0} \delta(x_i - x_{i0}) \delta(y_i - y_{i0}) \end{pmatrix}. \quad (20)$$

18 By substituting Eq. (8) into Eq. (20) and eliminating the position terms  $\cos \lambda_{iam} x_i$   
 19 and  $\cos \lambda_{ibn} y_i$ , the combined governing equations for all the I cells can be written in a  
 20 matrix form as

$$(\mathbf{Ra} + \mathbf{Sp}) - \omega^2 (\mathbf{Za} + \mathbf{Tp}) = \mathbf{F}, \quad (21)$$

where  $\mathbf{F} = [\mathbf{F}_0, \mathbf{F}_1, \dots, \mathbf{F}_l]^T$ , and  $\mathbf{F}_i$  are written as  $\mathbf{F}_i = [F_{i00}, F_{i01}, \dots, F_{i0N}, F_{i10}, F_{i11}, \dots, F_{i1N}, \dots, F_{iM0}, F_{iM1}, \dots, F_{iMN}]$ . The element  $F_{imn}$  in the force vector  $\mathbf{F}_i$  can be expressed as

$$F_{imn} = \frac{F_0}{\Lambda_{im}\Lambda_{in}} \cos \lambda_{im} x_{i0} \cos \lambda_{in} y_{i0}, \quad (22)$$

where  $\Lambda_{im} = \begin{cases} a_i & m=0 \\ a_i/2 & m \neq 0 \end{cases}$  and  $\Lambda_{in} = \begin{cases} b & n=0 \\ b/2 & n \neq 0 \end{cases}$ .

The vector  $\mathbf{P}$  in Eq. (21) can be eliminated by Eq. (19) where  $\mathbf{P}$  is expressed in terms of  $\mathbf{a}$ . Thus Eq. (21) can finally be given by

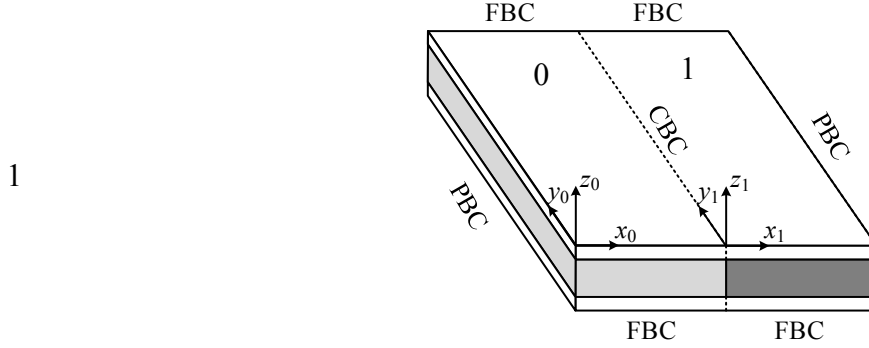
$$(\mathbf{K} - \omega^2 \mathbf{M}) \mathbf{a} = \mathbf{F}, \quad (23)$$

where  $\mathbf{K} = \mathbf{R} + \mathbf{S} \mathbf{H}^{-1} \mathbf{Q}$  and  $\mathbf{M} = \mathbf{Z} + \mathbf{T} \mathbf{H}^{-1} \mathbf{Q}$ .

For each given frequency  $\omega$ , the coefficient vector  $\mathbf{a}$  can be obtained by solving Eq. (23), and then  $\mathbf{P}$  can be determined by Eq. (19). With both unknown coefficient vectors  $\mathbf{a}$  and  $\mathbf{P}$ , the displacements of each sub sandwich plate can be acquired using Eq. (8), from which the forced response of a finite periodic sandwich plate can be finally determined and then the transmission characteristics can be examined analytically.

## 2.4 Band structure of an infinite periodic sandwich plate

The band structure of an infinite periodic sandwich plate can be determined by a unit element with Bloch-Floquet periodic boundary condition (PBC) [45]. Shown in **Fig. 6** is a unit element of the periodic sandwich plate with periodic boundary condition. As most of the calculating procedure for band-structure calculation is similar to the calculation of forced response, the calculating procedure is briefly discussed in this subsection.



2 **Fig. 6.** A unit element with periodic boundary condition.

3 The boundary equations of the FBCs along  $x$  direction ( $y_i = 0$  and  $y_i = b_i$ ) and the  
 4 boundary equations of the CBC are the same as they are given in Eqs. (15) and (17) in  
 5 subsection 2.3, except that the term  $i$  in Eq. (15) is limited to  $i = 0, 1$  and the term  $i$  in  
 6 Eq. (17) is limited to  $i = 1$  for the band-structure calculation in the present subsection.

7 According to Bloch-Floquet periodic condition, the boundary equations of the PBC  
 8 can be given as

$$9 \quad \begin{cases} u_{11}(a_1, y_1) = e^{jqa_L} u_{10}(0, y_0) & N_{11x}(a_1, y_1) = e^{jqa_L} N_{10x}(0, y_0) \\ v_{11}(a_1, y_1) = e^{jqa_L} v_{10}(0, y_0) & T_{11x}(a_1, y_1) = e^{jqa_L} T_{10x}(0, y_0) \\ u_{31}(a_1, y_1) = e^{jqa_L} u_{30}(0, y_0) & N_{31x}(a_1, y_1) = e^{jqa_L} N_{30x}(0, y_0) \\ v_{31}(a_1, y_1) = e^{jqa_L} v_{30}(0, y_0) & T_{31x}(a_1, y_1) = e^{jqa_L} T_{30x}(0, y_0) \\ w_1(a_1, y_1) = e^{jqa_L} w_0(0, y_0) & Q_{1x}(a_1, y_1) = e^{jqa_L} Q_{0x}(0, y_0) \\ \theta_1(a_1, y_1) = e^{jqa_L} \theta_0(0, y_0) & M_{1x}(a_1, y_1) = e^{jqa_L} M_{0x}(0, y_0) \end{cases}, \quad (24)$$

10 where  $q$  is Bloch wavenumber in  $x$  direction and  $a_L = a_0 + a_1$  is element length. By  
 11 taking the advantage of Eqs. (6) – (14) and following similar procedure described in  
 12 subsection 2.3, the combined boundary equation for band-structure calculation can be  
 13 arranged in a matrix form as

$$14 \quad \bar{\mathbf{H}}(q)\bar{\mathbf{p}} = \bar{\mathbf{Q}}(q)\bar{\mathbf{a}}, \quad (25)$$

15 where  $\bar{\mathbf{p}} = [\mathbf{p}_0, \mathbf{p}_1]^T$  and  $\bar{\mathbf{a}} = [\mathbf{a}_0, \mathbf{a}_1]^T$ . The expressions of  $\mathbf{p}_0$ ,  $\mathbf{p}_1$ ,  $\mathbf{a}_0$ , and  $\mathbf{a}_1$  have  
 16 been defined in Eq. (18). Multiplying an inverse matrix  $\bar{\mathbf{H}}(q)^{-1}$  at both sides of Eq. (25)

1 gives

2  $\bar{\mathbf{p}} = \bar{\mathbf{H}}(q)^{-1} \bar{\mathbf{Q}}(q) \bar{\mathbf{a}},$  (26)

3 which allows the expression of  $\bar{\mathbf{p}}$  in terms of  $\bar{\mathbf{a}}.$

4 After the boundary equations are obtained, the governing equations can be  
 5 determined by Eq. (20) with the force term  $F_{i0}\delta(x_i - x_{i0})\delta(y_i - y_{i0})$  being neglected and  
 6 the term  $i$  being limited to  $i = 0, 1.$  Then the combined governing equation can be  
 7 obtained in a matrix form as

8  $(\bar{\mathbf{R}}\bar{\mathbf{a}} + \bar{\mathbf{S}}\bar{\mathbf{p}}) - \omega^2 (\bar{\mathbf{Z}}\bar{\mathbf{a}} + \bar{\mathbf{T}}\bar{\mathbf{p}}) = \mathbf{0}.$  (27)

9 By substituting Eq. (26) into Eq. (27), Eq. (27) can be simplified to

10  $[\bar{\mathbf{K}}(q) - \omega^2 \bar{\mathbf{M}}(q)]\bar{\mathbf{a}} = \mathbf{0},$  (28)

11 where  $\bar{\mathbf{K}}(q) = \bar{\mathbf{R}} + \bar{\mathbf{S}}\bar{\mathbf{H}}(q)^{-1}\bar{\mathbf{Q}}(q)$  and  $\bar{\mathbf{M}}(q) = \bar{\mathbf{Z}} + \bar{\mathbf{T}}\bar{\mathbf{H}}(q)^{-1}\bar{\mathbf{Q}}(q).$

12 After solving Eq. (28), a set of characteristic frequencies can be obtained at a given  
 13 Bloch wavenumber  $q.$  By sweeping the normalized Bloch wavenumber  $q_n = qa_L/\pi$   
 14 from  $-1$  to  $+1$  in one period, the frequency-dependent dispersion curves of the possible  
 15 waves travelling in the periodic structure can be determined, which can give rise to the  
 16 band-gap properties of the periodic sandwich plate.

17 **3. Numerical results and discussion**

18 Both structural periodicity and damping have positive effect on the vibration  
 19 attenuation in a sandwich plate with viscoelastic periodic cores. To illustrate the band-gap  
 20 phenomenon arising from structural periodicity, the damping of sandwich cores A and B  
 21 are neglected firstly, as damping have some effect on the shape of dispersion curves and  
 22 make it difficult to determine the band-gap edge frequencies with damped dispersion  
 23 curves [43].

The bottom and top layers are selected as aluminum, and the soft core A and hard core B are polyurethane foam and thermoplastic rubber, respectively. The detailed information for dimensions and material parameters in a unit element is set in **Table 1** for further calculation. The parameters are kept unchanged in the following unless otherwise stated.

**Table 1** Dimensions and material parameters of a unit element.

	$E_s$ (GPa)	$G_s$ (GPa)	$\rho$ ( $\text{kg}\cdot\text{m}^{-3}$ )	$\nu$	$a$ (m)	$b$ (m)	$h$ (mm)
Bottom layer	77.6	28.7	2730	0.35	0.250	0.35	2.0
Core A	$1.38 \times 10^{-4}$	$5.11 \times 10^{-5}$	332	0.35	0.125	0.35	5.0
Core B	$2.50 \times 10^{-1}$	$8.39 \times 10^{-2}$	1100	0.49	0.125	0.35	5.0
Top layer	77.6	28.7	2730	0.35	0.250	0.35	1.8

Shown in **Fig. 7** is the band structure of an infinite periodic sandwich plate calculated by the theoretical model derived in subsection 2.4, together with the results calculated by FEM with the software of COMSOL Multiphysics. The excellent agreement between present model and FEM model provides validation for the theoretical model derived in this paper. From the band structure shown in **Fig. 7**, a band gap from 195.3 Hz to 286.0 Hz can be clearly observed in the shadow region, where none of dispersion curves is related to a given frequency and thus the flexural wave attenuates with increasing propagating distance.

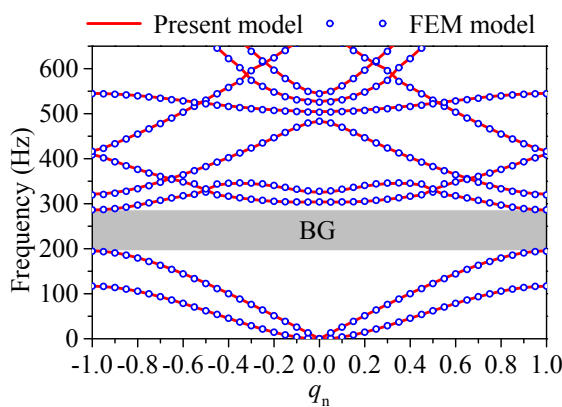


**Fig. 7.** Band structure in an infinite periodic sandwich plate. (BG: Band gap.)

The band-gap phenomenon in the periodic sandwich plate can be used to control vibration in plate structure, which can be proved by investigating the vibration transmission characteristics in a finite periodic sandwich plate. The configuration of the finite periodic structure considered in the following is shown in **Fig. 4**, and the number of element is chosen as four ( $I = 9$ ). A transverse harmonic point force is applied on the first sub sandwich plate (labelled with 0) at the position of ( $x_0 = 0.05$ ,  $y_0 = 0.09$ ). The spatially averaged transverse velocity of the last sub sandwich plate ( $\bar{v}_l$ ) is shown in **Fig. 8**. It can be seen in the figure that, out of the band gap (0 Hz – 195.3 Hz and 286.0 Hz – 650 Hz), the vibration response shows with large values, while in the band gap (195.3 Hz – 286.0 Hz), a response valley region shows up, where the flexural vibration of the last sub sandwich plate is significantly reduced. In **Fig. 8**, the velocity response is also calculated with FEM model, which shows that the two results have a good coincidence with each other, providing verification for the theoretical model in subsection 2.3.

14

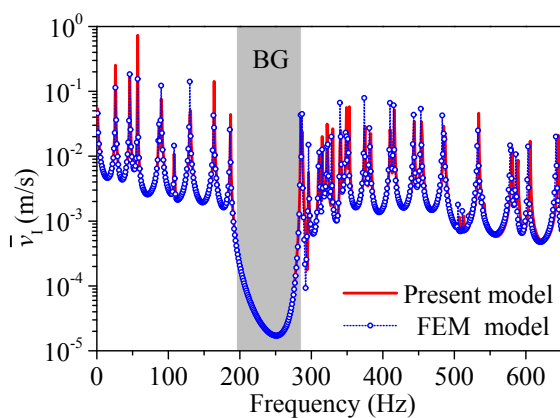


**Fig. 8.** Averaged velocity response of the last sub sandwich plate in a finite periodic sandwich plate. (BG: Band gap.)

Returning to **Fig. 7**, it is found that the band structure of the two-dimensional periodic sandwich plate is more complex than that of a corresponding one-dimensional periodic sandwich beam in Reference [43]. The independent dispersion branches may cross with each other in plate-type periodic sandwich structure. In the following, the

physical insight of the formation of the overall band gap in a periodic sandwich plate is further illustrated. As shown in **Fig. 7**, the band structure in a periodic sandwich plate consists of several independent dispersion branches and each branch corresponds to a specific wave-propagating mode. It is further found that the overall dispersion branches can be classified as several independent dispersion groups in terms of the cross-stream amplitude distribution in a unit element.

The overall dispersion branches below 900 Hz is shown in **Fig. 9(a)** and corresponding amplitude distributions of transverse displacement in a unit element for each dispersion branch at  $q_n = 0.75$  is shown in **Fig. 10**. By carefully observing the cross-stream amplitude distribution (along width/y direction) in **Fig. 10**, it can be obtained that five types of cross-stream modes are contained in the band structure in **Fig. 9(a)**. Thus the overall dispersion branches in **Fig. 9(a)** can be divided into five independent groups of dispersion branches, which are shown in **Fig. 9(b) – (f)**.

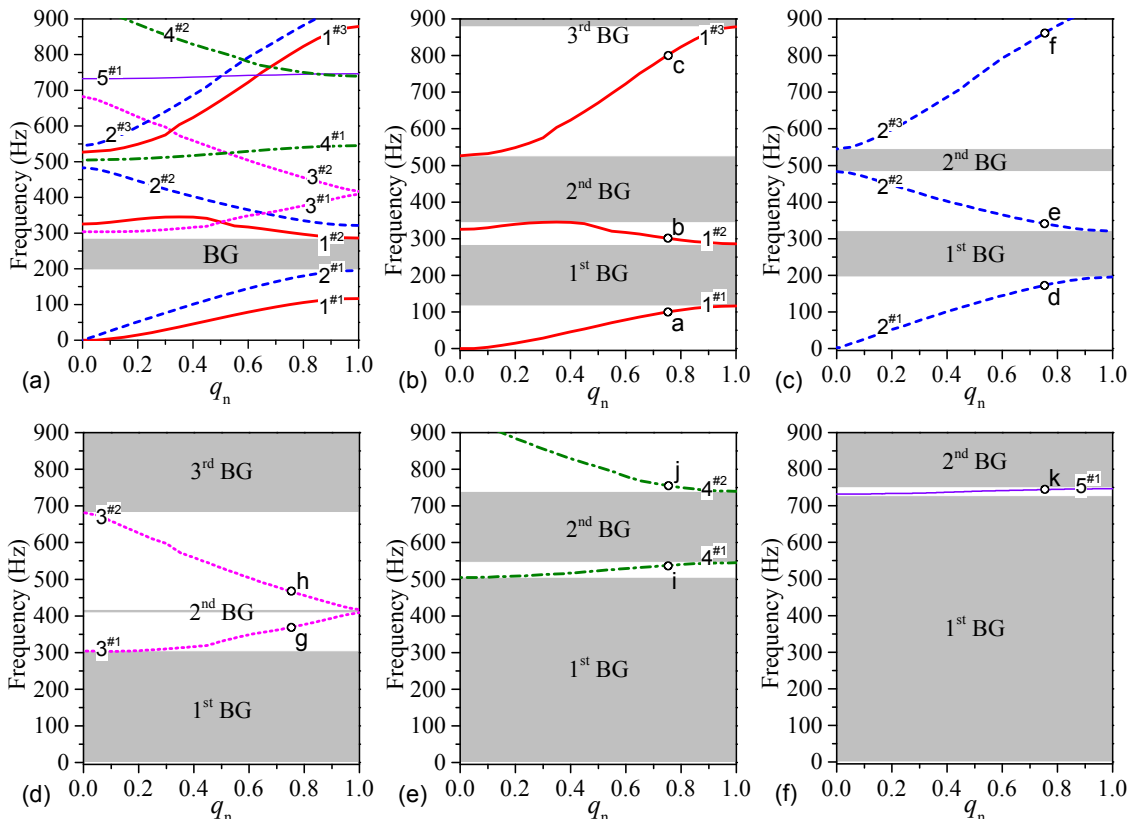
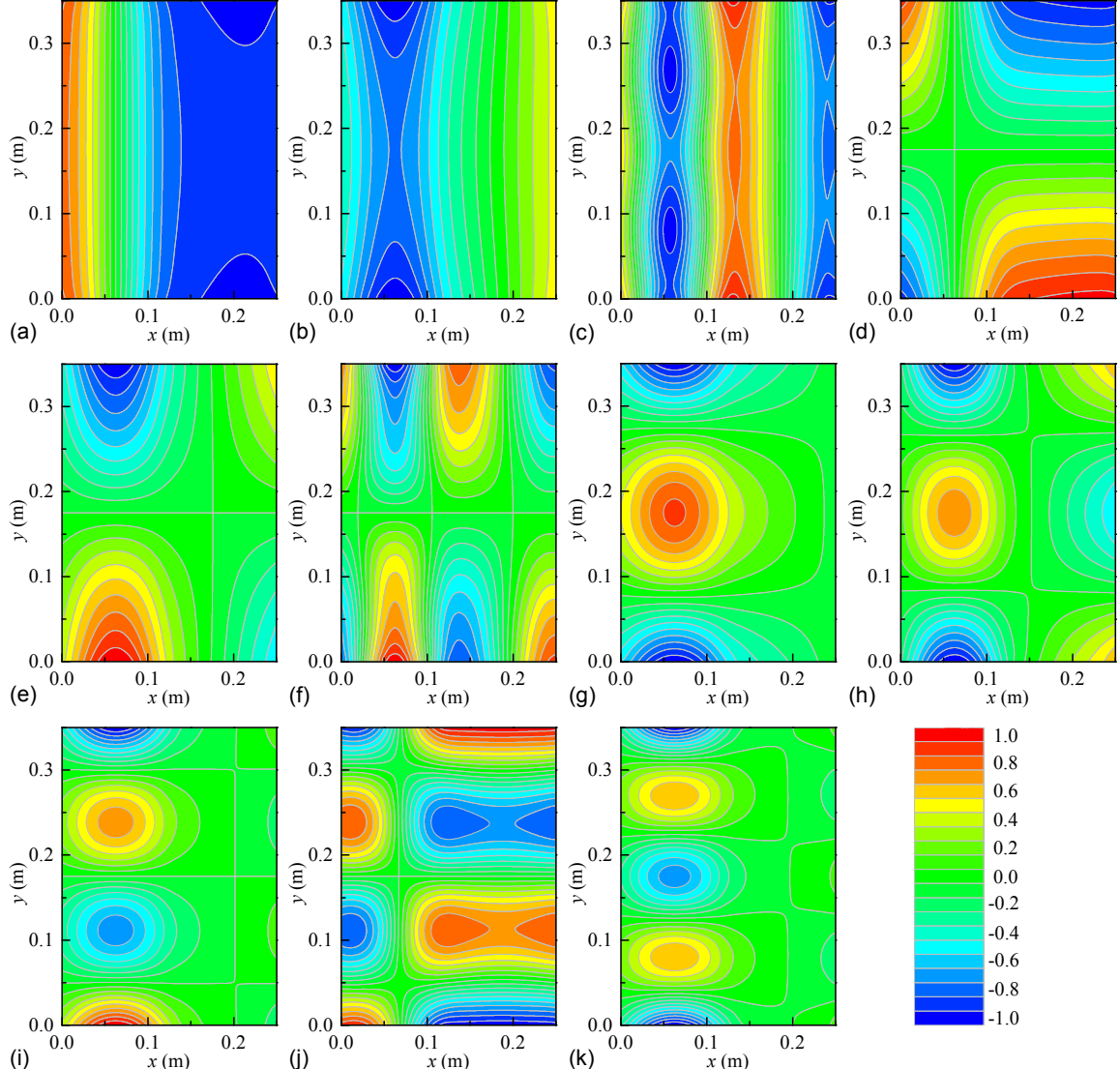


**Fig. 9.** (a) Overall dispersion branches and dispersion branches in the (b) first, (c) second,

1 (d) third, (e) fourth, and (f) fifth cross-stream modal groups. (BG: band gap; the letters  
 2 from ‘a’ to ‘k’ beside the circle ‘○’ denote the sub figure indices of **Fig. 10.**)



4 **Fig. 10.** Displacement amplitude distribution of a unit element at  $q_n = 0.75$  for the  
 5 dispersion branches in the first ((a)  $1^{\#1}$ , (b)  $1^{\#2}$ , and (c)  $1^{\#3}$ ), second ((d)  $2^{\#1}$ , (e)  $2^{\#2}$ , and (f)  
 6  $2^{\#3}$ ), third ((g)  $3^{\#1}$  and (h)  $3^{\#2}$ ), fourth ((i)  $4^{\#1}$  and (j)  $4^{\#2}$ ), and fifth ((k)  $5^{\#1}$ ) cross-stream  
 7 modal groups.

8 The amplitude distributions in **Fig. 10(a) – (c)** are related to dispersion branches  $1^{\#1}$ ,  
 9  $1^{\#2}$ , and  $1^{\#3}$  in **Fig. 9(b)**, which correspond to plane-wave propagation modes and are  
 10 denoted as the first cross-stream modal group. Those in **Fig. 10(d) – (f)** are related to  
 11 dispersion branches  $2^{\#1}$ ,  $2^{\#2}$ , and  $2^{\#3}$  in **Fig. 9(c)**, which correspond to the first anti-

1 symmetrical cross-stream modes and are classified as the second cross-stream modal  
 2 group. The same as the first and second cross-stream modal groups, the third, fourth, and  
 3 fifth cross-stream modal groups include dispersion branches 3<sup>#1</sup> and 3<sup>#2</sup> (see **Fig. 9(d)** and  
 4 **Fig. 10(g) – (h)**), dispersion branches 4<sup>#1</sup> and 4<sup>#2</sup> (see **Fig. 9(e)** and **Fig. 10(i) – (j)**), and  
 5 dispersion branch 5<sup>#1</sup> (see **Fig. 9(f)** and **Fig. 10(k)**), respectively. Thus the overall band  
 6 structure (**Fig. 9(a)**) below 900 Hz in a periodic sandwich plate can be considered as a  
 7 combination of each independent group of dispersion branches.

8 The dispersion branches of each cross-stream modal group constitute a band  
 9 structure for each cross-stream modal group as shown in **Fig. 9(b) – (f)**. In the following  
 10 statements, the band gaps existing in each cross-stream modal group are called as cross-  
 11 stream modal band gaps for convenient purpose. Thus the band gaps shown in **Fig. 9(b)** to  
 12 **Fig. 9(f)** correspond to the first to five cross-stream modal band gaps, respectively. Shown  
 13 in **Table 2** are the first five cross-stream modal band gaps and the overall band gaps  
 14 related to all the dispersion branches.

15 **Table 2** Overall band gap and cross-stream modal band gaps of a periodic sandwich plate.

	1 <sup>st</sup> modal group	2 <sup>nd</sup> modal group	3 <sup>rd</sup> modal group	4 <sup>th</sup> modal group	5 <sup>th</sup> modal group	Overall
1 <sup>st</sup> BG (Hz)	116.8–286.0	195.3–321.3	0–303.8	0–504.5	0–732.4	195.3–286.0
2 <sup>nd</sup> BG (Hz)	344.8–526.6	479.4–544.9	409.5–417.1	545.0–739.8	746.5–900	N/A
3 <sup>rd</sup> BG (Hz)	878.6–900	N/A	682.2–900	N/A	N/A	N/A

16  
 17 It can be observed in **Table 2** and **Fig. 9(b) – (f)** that the intersection of the first five  
 18 cross-stream modal band gaps can be evaluated by calculating the intersection of the  
 19 band-gap frequency regions 116.8 Hz – 286.0 Hz, 195.3 Hz – 321.3 Hz, 0 Hz – 303.8 Hz,  
 20 0 Hz – 504.5 Hz, and 0 Hz – 732.4 Hz. The intersection value can be finally obtained as  
 21 195.3 Hz – 286.0 Hz, which exactly equals to the overall band gap (195.3 Hz – 286.0 Hz)  
 22 in **Table 2**. Therefore, it can be determined that the overall band gap of a periodic

1 sandwich plate is the intersection of all the cross-stream modal band gaps. By  
2 understanding this phenomenon, we can further understand the difference of band-gap  
3 characteristics between a periodic sandwich plate and a periodic sandwich beam.

4 In fact, by comparing with the authors' previous research [43] for a sandwich beam  
5 with periodic cores, it is found that the overall dispersion branches in a periodic sandwich  
6 beam only correspond to the dispersion branches of the first cross-stream modal group  
7 (see **Fig. 9(b)**) in a periodic sandwich plate when the effect of Poisson's ratio is neglected.  
8 Thus, when one-dimensional periodic sandwich beam is extended to two-dimensional  
9 plate structure, more dispersion branches related to higher-order cross-stream modal  
10 groups are generated. This physical phenomenon results in reduced band-gap width in a  
11 periodic sandwich plate compared with a periodic sandwich beam. In a practical  
12 calculation, the band-gap width of the plate structure could be much smaller than the  
13 beam structure. For example, with the parameters shown in **Table 1**, the total band-gap  
14 width below 900 Hz in a periodic sandwich beam reaches 372.4 Hz, while that in a  
15 periodic sandwich plate reduces remarkably to 90.7 Hz, which is less than a quarter of that  
16 in beam structure. Thus, the band-gap design for a periodic sandwich plate could be much  
17 more difficult. In the following parametric analysis, it is even found that the overall band  
18 gap in a periodic sandwich plate may disappear when the parameters are improperly  
19 selected, which does not happen in a periodic sandwich beam.

20 In order to obtain more detailed band-gap characteristics of the periodic sandwich  
21 plate, the effects of dimensional parameters on band-gap frequency and band-gap width  
22 are further examined, including the parameters of element length  $a_L$ , length ratio  
23  $\alpha = a_A/a_B$  ( $A$  is soft core and  $B$  is hard core), element width  $b$ , and core thickness  $h_c$ .  
24 For each specific parametric analysis, the other parameters are kept unchanged as listed in  
25 **Table 1**. The results of the dimensional parametric analysis are shown in **Fig. 11**.

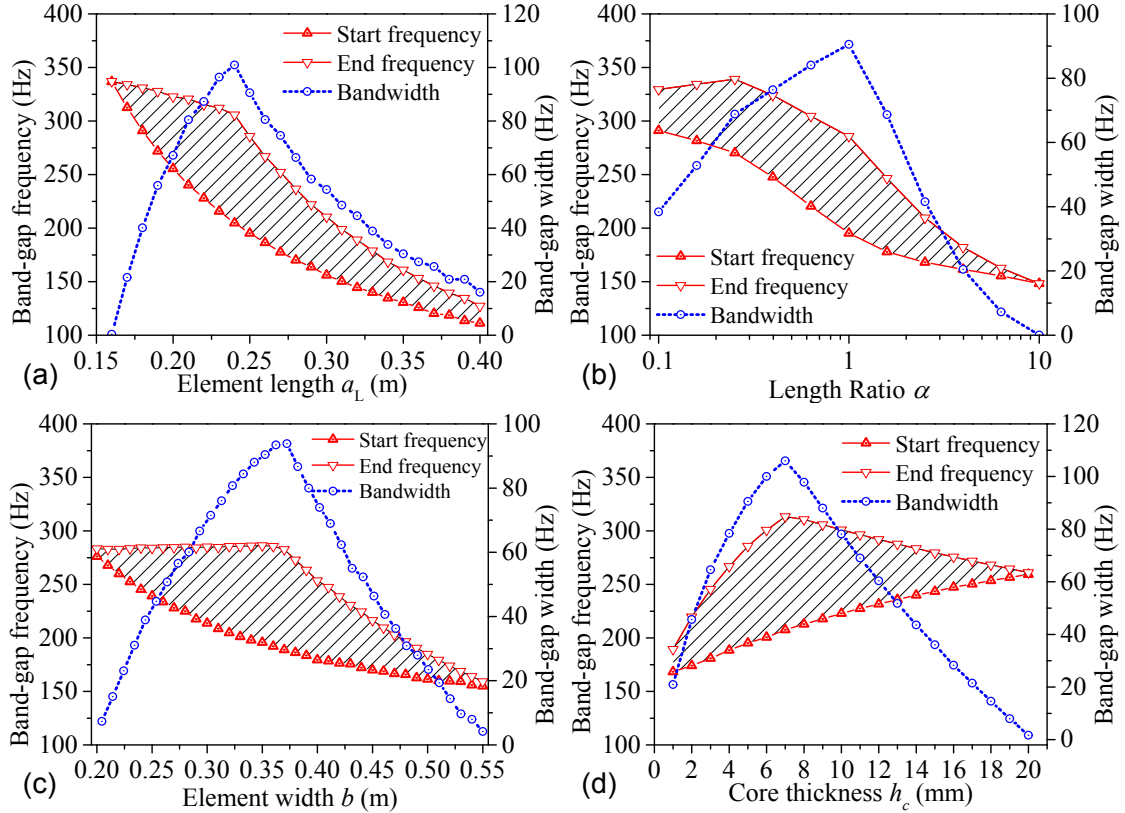


**Fig. 11.** Effects of dimensional parameters of (a) element length, (b) length ratio, (c) element width, and (d) core thickness on band-gap frequency and band-gap width.

The element length  $a_L$  is set to vary from 0.16 m to 0.40 m with  $a_A = a_B$ . As shown in **Fig. 11(a)**, with the increase of  $a_L$ , the band-gap frequency decreases, which is quite normal, as longer cell can attenuate longer-wavelength flexural wave due to Bragg scattering mechanism. Thus the variation of band-gap frequency in a periodic sandwich plate is consistent with that in a periodic sandwich beam. For the band-gap width, with the increase of element length  $a_L$ , it first increases and then decreases, reaching a maximum value 100.9 Hz at  $a_L = 0.24$  m. This variation of band-gap width is quite different from the beam structure, where an increased element length is always related to a decreased band-gap width. This difference between beam and plate structure is due to the band-gap formation of plate structure, whose overall band gaps are formed by the intersection of all the cross-stream modal band gaps. For each cross-stream modal group, an increased element length is still related to a decreased cross-stream model band-gap width. However,

1 for the intersection of all the cross-stream modal band gaps, the monotonic variation does  
2 not work out.

3 As shown in **Fig. 11(b) – (d)**, for the parameters of length ratio  $\alpha$ , element width  $b$ ,  
4 and core thickness  $h_c$ , the variation of band-gap width shows similar tendency to the  
5 parameter of element length  $a_L$  (**Fig. 11(a)**), where band-gap width first increases and  
6 then decreases with increasing parameter, reaching maximum at the optimized position. It  
7 can be observed that the maximum positions for length ratio, element width, and core  
8 thickness can be obtained respectively at  $\alpha = 1$ ,  $b = 0.37\text{ m}$ , and  $h_c = 7\text{ mm}$ , with the  
9 maximum band-gap widths reaching 90.5 Hz, 93.8 Hz, and 105.9 Hz, respectively. In the  
10 design of a periodic sandwich plate, the attenuation performance can be improved when  
11 these parameters are tuned at these optimized positions. It should be also observed that the  
12 band gap of a periodic sandwich plate could disappear when length ratio, element width,  
13 or core thickness exceeds a specific (cut-off) value. As shown in **Fig. 11(b) – (d)**, when  
14  $\alpha > 10$ ,  $b > 0.55\text{ m}$ , or  $h_c > 20\text{ mm}$ , the band-gap width becomes zero and the band gap  
15 disappears. This phenomenon is quite different from a periodic sandwich beam [43],  
16 where dimensional parameters only have effect on band-gap location and band-gap width,  
17 yet the band gap always exists. This band-gap disappearing phenomenon is also caused by  
18 the complex band-gap formation mechanism, where overall band gaps are formed by the  
19 intersection of all the cross-stream modal band gaps. With the variation of dimensional  
20 parameters, the cross-stream modal band gaps would not disappear. However, the  
21 intersection of all the cross-stream modal band gaps could possibly disappear due to the  
22 complex effect of parameters on all the dispersion branches related to all the cross-stream  
23 modal groups. Therefore, care should be taken in a structure design, where the parameters  
24 of length ratio, element width, and core thickness should not exceed the cut-off values to  
25 prevent the band gap disappearing.

Apart from the dimensional parameters, the material parameters also have effect on band-gap characteristics, especially the parameter of Young's modulus, as it can provides marked difference between soft core and hard core when the materials of periodic cores are properly selected. The independent effect of Young's modulus of soft core and that of hard core are shown in **Fig. 12(a)** and **Fig. 12(b)**, respectively. When one of the Young's modulus varies, the other one keeps unchanged as shown in **Table 1**, where the Young's moduli of soft core  $E_A$  and hard core  $E_B$  are initially set as  $E_A = 1.38 \times 10^5$  Pa and  $E_B = 2.5 \times 10^8$  Pa, respectively.

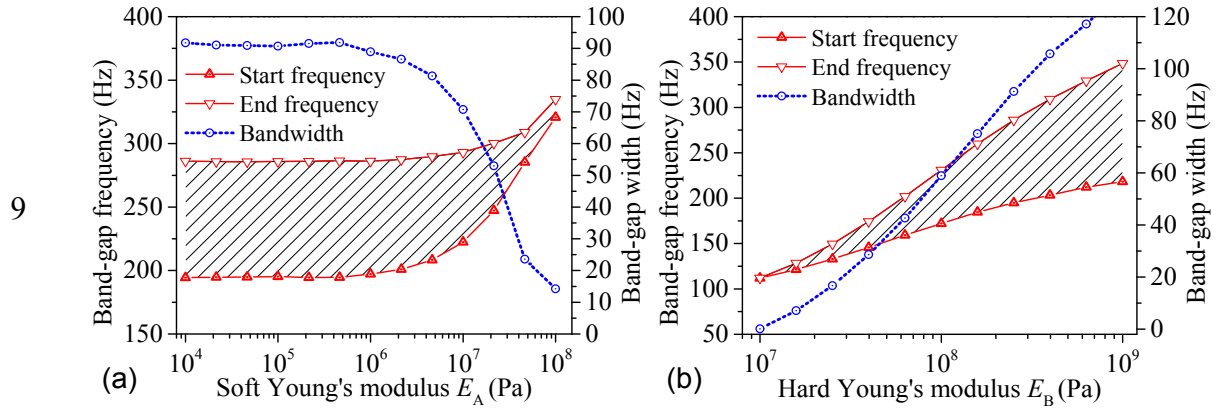


**Fig. 12.** Effects of (a) Young's modulus of soft core  $E_A$  and (b) Young's modulus of hard core  $E_B$  on band-gap frequency and band-gap width.

It can be seen in **Fig. 12** that, with the increase of  $E_A$  or  $E_B$ , the band-gap frequencies increase, as the increasing Young's modulus will increase the overall bending stiffness of a periodic sandwich plate, which results in increasing characteristic frequencies. On the other hand, the band-gap width decreases with increasing Young's modulus of soft core  $E_A$  (see **Fig. 12(a)**) and increases with increasing Young's modulus of hard core  $E_B$  (see **Fig. 12(b)**), implying that increasing the difference between  $E_A$  and  $E_B$  will increase the band-gap width.

In the above, the damping of viscoelastic periodic cores is neglected to analyze the

band-gap characteristics of a periodic sandwich plate. It is found that, in the band gap, the vibration can be significantly reduced (see **Fig. 8**). However, strong vibration still shows up at the frequency out of the band gap. In the following, the effect of damping in periodic cores on vibration-reduction performance is further analyzed.

For a specific material, the material loss factor  $\eta$  can be frequency dependent, and its value can be determined by damping experiment. In the following numerical analysis,  $\eta$  is considered as frequency independent as the values specified in the analysis are only used for convenient and qualitative comparison purpose. Other dimensions and material parameters used in the following keep the same as those used in the previous undamped case for a finite periodic sandwich plate. In this examination, the damping of core A (soft core) and core B (hard core) are assumed to be identical, *i.e.*,  $\eta_A = \eta_B = \eta$ , for convenient purpose. The effect of damping on the vibration-reduction performance of a finite periodic sandwich plate is shown in **Fig. 13**, where the averaged velocity response of the last sub sandwich plate ( $\bar{v}_l$ ) is given and the loss factor varies from zero to 0.30.

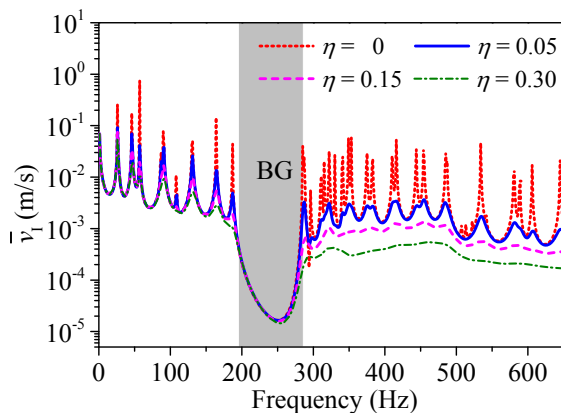


**Fig. 13.** Effect of damping on averaged velocity response of the last sub sandwich plate.

It can be seen in **Fig. 13** that the vibration response in the band gap is hardly affected by damping, while out of the band gap, especially above the band gap, damping has significant effect on vibration response. In the frequency range out of the band gap (0 Hz – 195.3 Hz and 286.0 Hz – 650 Hz), the velocity response of the last sub sandwich

plate decreases with the increase of loss factor  $\eta$ , showing that damping has positive effect on vibration reduction in the pass bands.

From the above study, it can be determined that two attenuation mechanisms can be found in a sandwich plate with viscoelastic periodic cores, including Bragg scattering mechanism arising from structural periodicity and energy dissipation mechanism arising from material damping of the periodic cores. In the band gap, the attenuation is dominated by Bragg scattering mechanism, while out of the band gap, it is mainly controlled by energy dissipation mechanism. Thus the sandwich plate with viscoelastic periodic cores has attractive characteristics of reducing flexural-wave energy at most frequencies, as the waves in the band gap can be attenuated by Bragg scattering and the waves in the pass bands can be attenuated by damping. As shown in **Fig. 13**, all the flexural wave components are reduced not only in the band gap but also in the pass bands above approximately 150 Hz for the case of  $\eta = 0.15$ .

In order to study the damping effect of independent soft core (core A) and independent hard core (core B) on attenuation performance, four more cases are further examined with case 1:  $\eta_A = \eta_B = 0$ ; case 2:  $\eta_A = 0.15$  and  $\eta_B = 0$ ; case 3:  $\eta_A = 0$  and  $\eta_B = 0.15$ ; and case 4:  $\eta_A = \eta_B = 0.15$ . The averaged velocity response of the last sub sandwich plate for these four cases are shown in **Fig. 14** for further comparison.

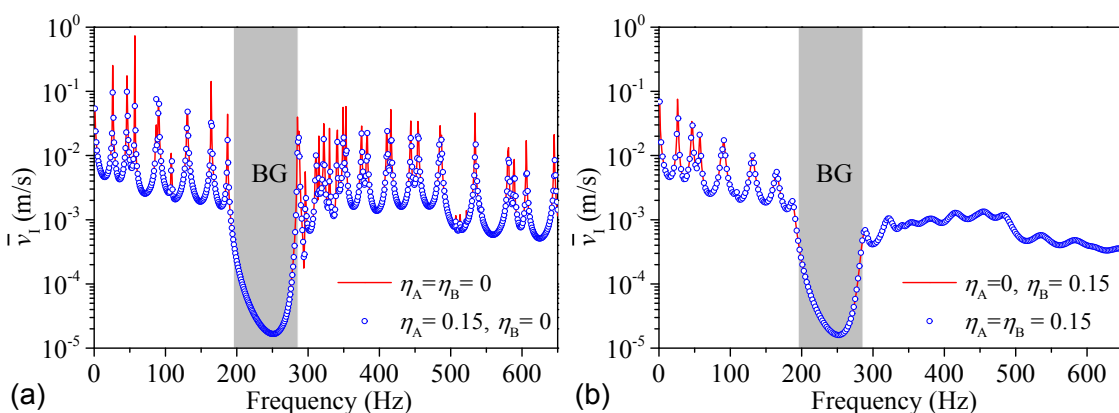


**Fig. 14.** Damping effect of independent soft core (core A) and independent hard core

1 (core B) on vibration response with (a) comparison between case 1 and case 2 and (b)  
2 comparison between case 3 and case 4.

3 It can be seen from **Fig. 14(a)** that, when the damping of hard core (core B) is  
4 neglected, the damping change of soft core (core A) has very limited effect on the  
5 vibration response. For the damped case 2  $\eta_A = 0.15$  and  $\eta_B = 0$ , the vibration response  
6 still shows large values out of the band gap. However, for the damped case 3  $\eta_A = 0$  and  
7  $\eta_B = 0.15$  in **Fig. 14(b)**, where the damping of soft core (core A) is neglected, the  
8 vibration response out of the band gap is significantly reduced. As shown in **Fig. 14(b)**,  
9 the vibration response of case 3 nearly coincides with that of the double damped case 4.  
10 Thus, it can be inferred from the above comparison results that the damping effect in the  
11 periodic sandwich plate is mainly induced by the hard viscoelastic core and the damping  
12 of the soft viscoelastic core has very limited effect on reducing vibration response.  
13 Therefore, to improve the attenuation performance in a periodic sandwich plate design,  
14 tuning damping of the hard core will be much more effective than tuning that of the soft  
15 core. It also implies that the soft core could be selected as soft elastic material in addition  
16 to soft viscoelastic material.

17 In the following, the attenuation performance of a sandwich plate with viscoelastic  
18 peirodic cores is compared with that of a sandwich plate with corresponding viscoelastic  
19 uniform soft core or uniform hard core. For the periodic sandwich plate, the dimensions  
20 and materials keep unchanged as previous numerical examples, except that the loss factors  
21 of the cores are set as  $\eta_A = \eta_B = 0.15$ . The materials of uniform soft core and uniform  
22 hard core in the two uniform sandwich plates are the same as the materials of core A and  
23 core B in the periodic sandwich plate, respectively. Other dimensions and material  
24 parameters of these three sandwich plates keep the same. The averaged velocity responses  
25 of the last sub sandwich plate in the above three sandwich plates are shown in **Fig. 15**.

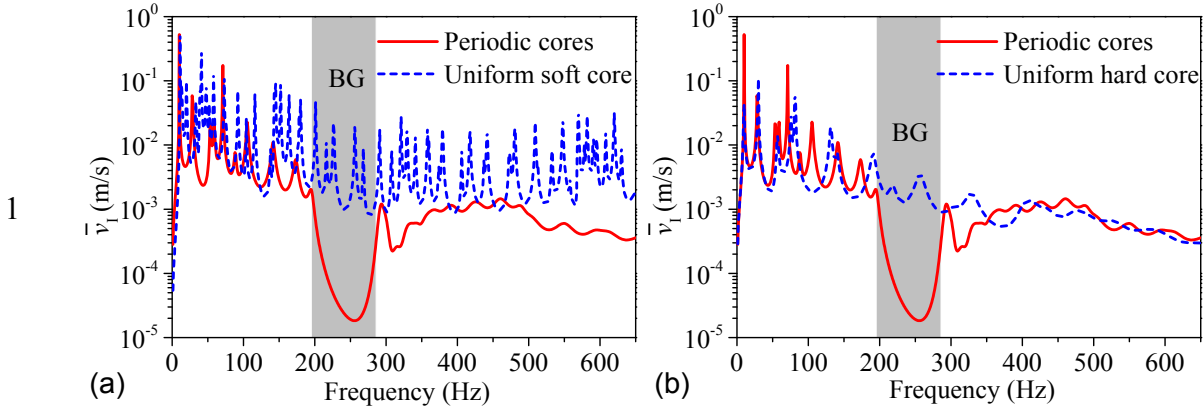


**Fig. 15.** Comparisons of averaged velocity response of the last sub sandwich plate among three sandwich plates with (a) comparison between periodic cores and uniform soft core and (b) comparison between periodic cores and uniform hard core.

It can be seen in **Fig. 15(a)** that the vibration response of the sandwich plate with viscoelastic periodic cores is much smaller than the sandwich plate with viscoelastic uniform soft core at almost all the considered frequencies, which owns to both the bandgap phenomenon and the damping of the periodic cores in the periodic structure. It can also be observed in **Fig. 15(b)** that, in the frequency range out of the band gap, the sandwich plate with viscoelastic periodic cores has comparable vibration response to the uniform structure with viscoelastic hard core due to comparable damping effect. However, in the band gap, the vibration response of the periodic structure is much smaller than that of the structure with uniform hard core, with an average attenuation level more than 25 dB.

Therefore, from the above examinations, it can be found that the sandwich plate with viscoelastic periodic cores shows better performance in vibration attenuation than that with viscoelastic uniform cores in band gap. Generally, the sandwich plate with viscoelastic uniform core is called as CLD structure, which is used as a common approach to reduce structure vibration. From the above study, it can be inferred that the CLD structure can be improved by replacing the viscoelastic uniform core with viscoelastic periodic cores, which improves the vibration-reduction performance due to the combined

attenuation mechanism of both Bragg scattering and damping. The improved damping structure can be called as PCLD structure [43], providing a new better approach for designing damping structures.

#### 4. Experimental results

In order to verify the analytical model and numerical results, a sandwich plate specimen with viscoelastic periodic cores was fabricated and tested. The two identical surface layers of the specimen were made of aluminum with the dimension of 1390 mm×380 mm×1.85 mm. Shown in **Fig. 16** are the periodic cores of the sandwich plate, where the two periodic cores were made of foam and polymethyl methacrylate (PMMA). Core A and core B had the same dimensions, with length 120 mm, width 380 mm, and thickness 5 mm. The finite periodic sandwich plate can be considered as twelve sub sandwich plates joining together end to end, where the length of the left-end sub sandwich plate (labelled as 0) was 70 mm, while the length of the other eleven sub sandwich plates were 120 mm. The Young's moduli and densities of both foam and PMMA were tested and measured as  $E_A = 5.8 \times 10^5 \text{ Pa}$ ,  $\rho_A = 54.9 \text{ kg/m}^3$ ,  $E_B = 2.2 \times 10^9 \text{ Pa}$ , and  $\rho_B = 1153.1 \text{ kg/m}^3$ , respectively.

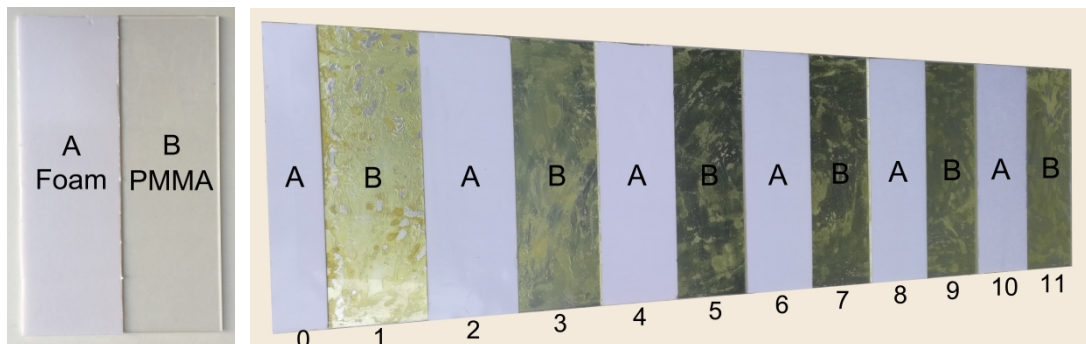
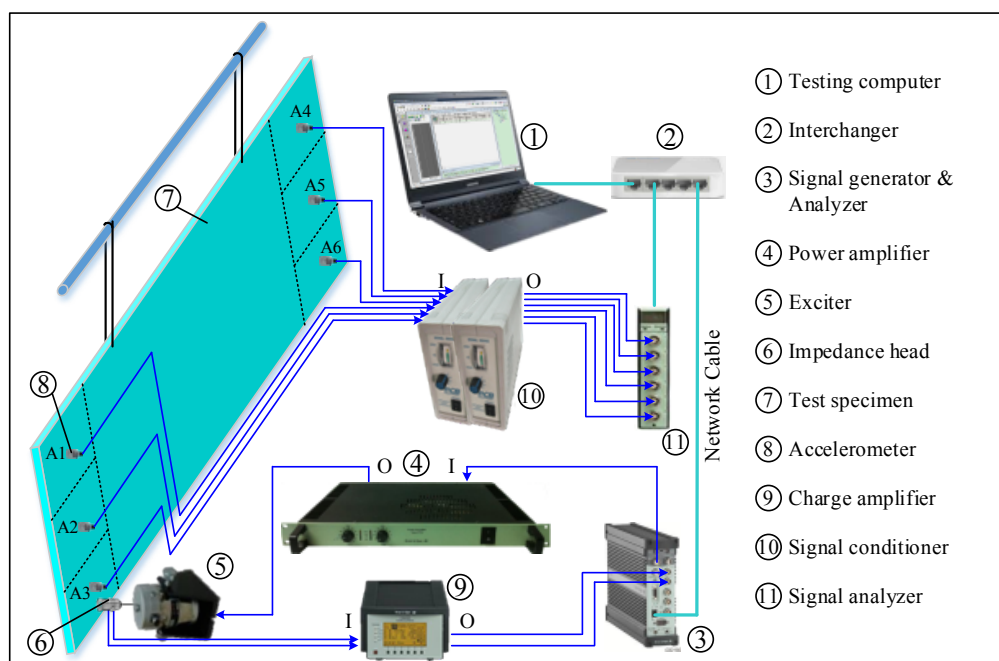


**Fig. 16.** Periodic cores of the tested sandwich plate.

The schematic diagram of experimental set-up and the practical experimental set-up are shown in **Fig. 17** and **Fig. 18**, respectively. The periodic sandwich plate was suspended by two elastic ropes to approximately simulate the free boundary condition. An

1 excitation signal generated by signal generator & analyzer was transferred to a vibration  
 2 exciter after power amplification by a power amplifier. An impedance head was mounted  
 3 on the exciter to measure its input acceleration and input force, which were analyzed by  
 4 signal analyzer after charge signal was transformed to voltage signal by charger amplifier.  
 5 The input force acquired by impedance head was used as a reference signal in the process  
 6 of data analysis. The excitation position was located at ( $x = 0.06\text{ m}$ ,  $y = 0.085\text{ m}$ ) with  
 7 the left down corner considered as the original point. In order to illustrate the band-gap  
 8 phenomenon of periodic sandwich plate, three accelerometers were mounted at the left-  
 9 end region (A1, A2, and A3 near excitation position) of the sandwich plate and the other  
 10 three were mounted at the right-end region (A4, A5, and A6 far from excitation position).  
 11 These six acceleration signals were firstly transferred to two signal conditioners and then  
 12 transferred to a signal analyzer. The experimental data collected from the set-up was  
 13 processed finally by the testing software PULSE Labshop in a testing computing.

14



15

**Fig. 17.** Schematic diagram of experimental set-up.

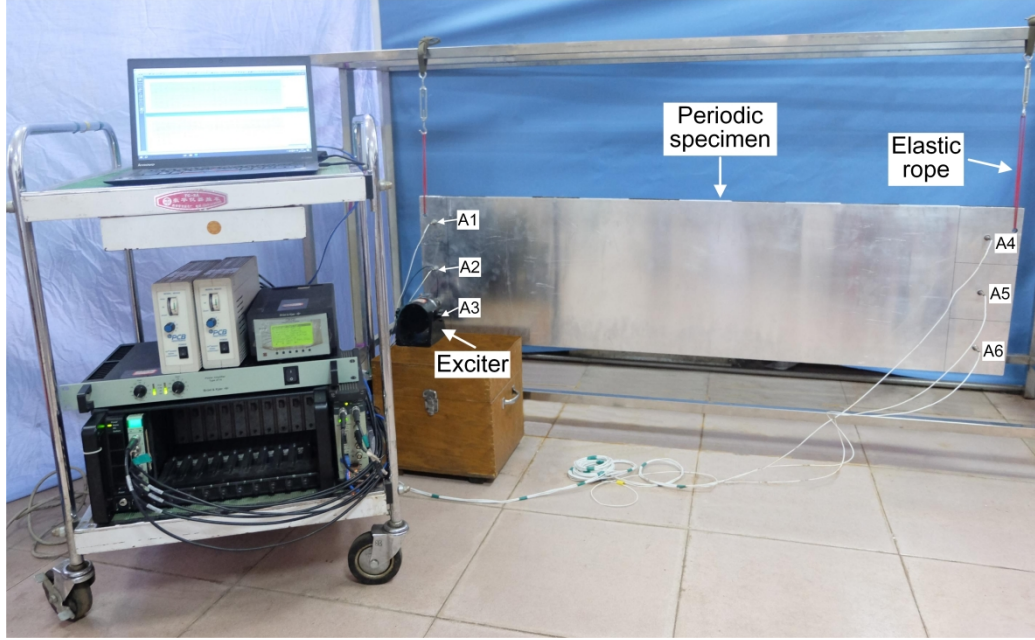


**Fig. 18.** Practical experimental set-up.

In order to clearly illustrate the band-gap phenomenon in the periodic sandwich plate, the accelerations of signals A1, A2, and A3 in the left-end region (near excitation place) were averaged and normalized by the input force  $f_0$ . The normalized average acceleration level of the left-end region is expressed as

$$\bar{L}_{a0} = 20 \lg \left[ \frac{1}{3} \sum_{i=1}^3 a_i^2 / (a_{\text{ref}}^2 f_0^2) \right], \quad (29)$$

where  $a_{\text{ref}} = 1 \times 10^{-6}$  m/s and  $a_i$  ( $i = 1, 2, 3$ ) represents the acceleration of signal A1, A2, or A3 near excitation. On the other hand, the normalized average acceleration level of the right-end region is expressed as

$$\bar{L}_{a1} = 20 \lg \left[ \frac{1}{3} \sum_{i=4}^6 a_i^2 / (a_{\text{ref}}^2 f_0^2) \right], \quad (30)$$

where  $a_i$  ( $i = 4, 5, 6$ ) represents the acceleration of signal A4, A5, or A6, which locates at the right-end region far from the excitation. The vibration responses of  $\bar{L}_{a0}$  and  $\bar{L}_{a1}$  in the periodic sandwich specimen are compared in Fig. 19.

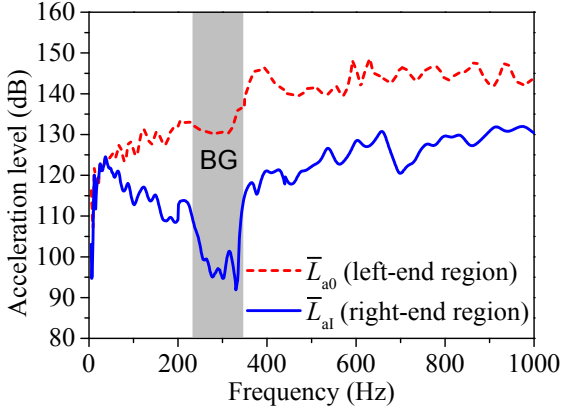


**Fig. 19.** Comparison of average responses between the left-end region and right-end region in the sandwich specimen. (BG: band gap.)

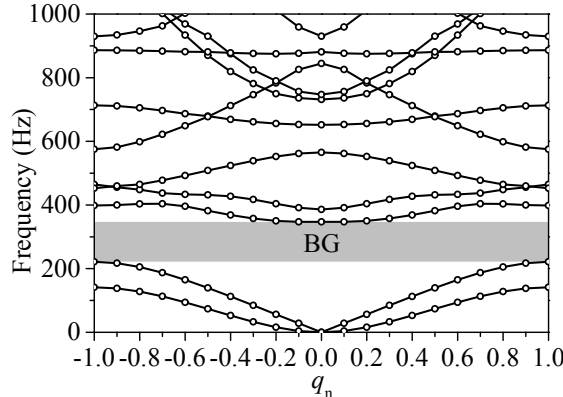
By comparing the two curves of  $\bar{L}_{a0}$  and  $\bar{L}_{al}$  in **Fig. 19**, it can be seen that  $\bar{L}_{al}$  is much smaller than  $\bar{L}_{a0}$  in the frequency range from approximately 50 Hz to 1000 Hz, which means that the flexural wave is attenuated in a broad band when propagating from the left-end region to the right-end region. This attenuation is resulted by both energy dissipation arising from the cores' damping and Bragg scattering arising from the periodic cores.

By further observing the curve  $\bar{L}_{al}$ , it can also be found that a vibration valley exists in the frequency range from approximately 220 Hz to approximately 350 Hz, which means that a band gap has generated in this frequency range. The vibration-reduction performance of the periodic sandwich specimen is improved in the band-gap frequency compared with the frequency out of band gap, with approximately more than 17 dB additional attenuation.

The band structure of the experimental specimen is also calculated by the analytical model derived in subsection 2.4, as shown in **Fig. 20**. In the figure, a band gap from 221.6 Hz to 346.9 Hz can be clearly observed. It can be further found that the frequency range of the vibration valley tested in the experiment in **Fig. 19** has a good coincidence with the band gap calculated by the present analytical model in **Fig. 20**, which provides an

1 experimental verification for the theoretical model derived in this paper.

2



3 **Fig. 20.** Band structure calculated by present analytical model. (BG: band gap.)

4 **5. Conclusions**

5 The flexural vibration behavior of a sandwich plate with viscoelastic periodic cores  
6 was examined analytically and experimentally in this paper, which thoroughly extended  
7 the previous research of corresponding periodic sandwich beam structure.

8 The band structure of a sandwich plate with periodic cores can be classified as  
9 several independent groups of dispersion branches in terms of the cross-stream amplitude  
10 distribution. Thus the overall band gap is proved to be the intersection of all the  
11 independent cross-stream modal band gaps, which is different from a periodic sandwich  
12 beam. It is further found that the overall band gap of beam structure is the first cross-  
13 stream modal band gap of the corresponding plate structure, implying that the band-gap  
14 width of a two-dimensional periodic sandwich plate could be much smaller than the  
15 corresponding one-dimensional beam structure and its band-gap design could be more  
16 complicated.

17 With the increase of element length, length ratio, element width, or core thickness,  
18 the band-gap width first increases and then decreases, reaching maximum at an optimized  
19 value, implying that tuning these parameters at the optimized values could maximize the  
20 band-gap width in the desired frequency range. Furthermore, the band gap could

1 disappear when length ratio, element width, or core thickness exceeds a cut-off value.  
2 Therefore, care should be taken in a band-gap design, where the parameters of length ratio,  
3 element width, and core thickness should not exceed the cut-off value to prevent the band  
4 gap disappearing.

5 The overall attenuation performance of a sandwich plate with viscoelastic periodic  
6 cores is affected by both energy dissipation mechanism arising from cores' damping and  
7 Bragg scattering mechanism arising from structure periodicity. The attenuation  
8 performance is mainly dominated by Bragg scattering in the band gap and by energy  
9 dissipation out of the band gap. Owing to the combined effect of both mechanisms, the  
10 plate with periodic constrained-layer damping treatment shows better performance than  
11 that with the traditional constrained-layer damping treatment. Thus, the sandwich plate  
12 with viscoelastic periodic cores can be considered as a new improved plate-type damping  
13 structure.

14 This work is limited to a sandwich plate with viscoelastic periodic cores and is based  
15 on the authors' previous study for a corresponding periodic sandwich beam structure. This  
16 work can be further extended to a periodic sandwich shell structure, which may provide  
17 more useful guidance on the design of periodic damping structures and also on vibration  
18 control in more practical sandwich structures.

## 19 **Acknowledgements**

20 The authors gratefully acknowledge the financial support from Shenzhen Science  
21 and Technology Innovation Committee (JCYJ20170306154350796).

## 22 **Appendix A**

23 The differential operators  $L_{ij}$  ( $i, j = 1, \dots, 5$ ) in Eq. (5) can be expressed as

24 
$$L_{11} = -B_1 \frac{\partial^2}{\partial x^2} - \nu_{1a} B_1 \frac{\partial^2}{\partial y^2} + G_h - \omega^2 (m_1 + 2C), \quad (\text{A.32})$$

$$L_{12} = L_{21} = -\nu_{lb} B_1 \frac{\partial^2}{\partial x \partial y}, \quad (\text{A.33})$$

$$2 \quad L_{13} = L_{31} = -G_h - \omega^2 C, \quad (\text{A.34})$$

$$3 \quad L_{14} = L_{41} = L_{23} = L_{32} = 0, \quad (\text{A.35})$$

$$4 \quad L_{15} = -G_h d \frac{\partial}{\partial x} - 6\omega^2 C h_{t1} \frac{\partial}{\partial x}, \quad (\text{A.36})$$

$$5 \quad L_{22} = -\nu_{1a} B_1 \frac{\partial^2}{\partial x^2} - B_1 \frac{\partial^2}{\partial y^2} + G_h - \omega^2 (m_1 + 2C), \quad (\text{A.37})$$

$$6 \quad L_{24} = L_{42} = -G_h - \omega^2 C, \quad (\text{A.38})$$

$$L_{25} = L_{52} = -G_h d \frac{\partial}{\partial y} - 6\omega^2 C h_{t1} \frac{\partial}{\partial y}, \quad (\text{A.39})$$

$$8 \quad L_{33} = -B_3 \frac{\partial^2}{\partial x^2} - v_{3a} B_3 \frac{\partial^2}{\partial y^2} + G_h - \omega^2 (m_3 + 2C), \quad (\text{A.40})$$

$$L_{34} = L_{43} = -v_{3b} B_3 \frac{\partial^2}{\partial x \partial y}, \quad (\text{A.41})$$

$$L_{35} = L_{53} = G_h d \frac{\partial}{\partial x} - 6\omega^2 C h_{t2} \frac{\partial}{\partial x}, \quad (\text{A.42})$$

$$L_{44} = -\nu_{3a} B_3 \frac{\partial^2}{\partial x^2} - B_3 \frac{\partial^2}{\partial y^2} + G_h - \omega^2 (m_3 + 2C), \quad (\text{A.43})$$

$$L_{45} = L_{54} = G_h d \frac{\partial}{\partial y} - 6\omega^2 C h_{t2} \frac{\partial}{\partial y}, \quad (\text{A.44})$$

13 and

$$L_{55} = -\left(D_1 + D_3\right)\left(\frac{\partial^2}{\partial x^2} + \frac{\partial^2}{\partial y^2}\right)^2 + G_h d^2 \left(\frac{\partial^2}{\partial x^2} + \frac{\partial^2}{\partial y^2}\right) + \omega^2 \left[m_T - \left(J_1 + J_3 + m_2 h_{i3}\right)\left(\frac{\partial^2}{\partial x^2} + \frac{\partial^2}{\partial y^2}\right)\right], \quad (A.45)$$

15 where,  $h_{t1} = (h_3 - 2h_1)/12$ ,  $h_{t2} = (2h_3 - h_1)/12$ ,  $h_{t3} = (h_3 - h_1)^2/16 + (h_1 + h_3)^2/48$ ,

1       $m_T = \sum_{i=1}^3 \rho_i h_i$ ,  $\nu_{ib} = (1 + \nu_i)/2$ , and  $C = m_2/6$ .

2      The matrices  $\mathbf{B}_{is0}$  to  $\mathbf{B}_{is4}$  used in Eq. (11) can be expressed as

3      
$$\mathbf{B}_{is0} = \begin{bmatrix} 0 & 1 & 0 & 0 \\ 1 & 0 & 0 & 0 \\ 0 & 0 & 0 & 1 \\ 0 & 0 & 1 & 0 \end{bmatrix}, \quad (\text{A.46})$$

4      
$$\mathbf{B}_{is1} = \frac{\pi}{2s_i} \text{diag}(1 \ -1 \ 3 \ -3), \quad (\text{A.47})$$

5      
$$\mathbf{B}_{is2} = \frac{\pi^2}{4s_i^2} \text{diag}(-1 \ -1 \ -9 \ -9), \quad (\text{A.48})$$

6      
$$\mathbf{B}_{is3} = \frac{\pi^3}{8s_i^3} \text{diag}(-1 \ 1 \ -27 \ 27), \quad (\text{A.49})$$

7      and

8      
$$\mathbf{B}_{is4} = \frac{\pi^4}{16s_i^4} \text{diag}(1 \ 1 \ 81 \ 81). \quad (\text{A.50})$$

9      The term  $\tau_r$  in Eq. (12) can be expressed as

10     
$$\tau_r = [\tau_r^1 \ \tau_r^2 \ \tau_r^3 \ \tau_r^4]^T = \begin{cases} \left[ \begin{array}{cccc} \frac{2}{\pi} & \frac{2}{\pi} & \frac{2}{3\pi} & -\frac{2}{3\pi} \end{array} \right]^T & r=0 \\ \left[ \begin{array}{cccc} \frac{4}{(1-4r^2)\pi} & \frac{4(-1)^r}{(1-4r^2)\pi} & \frac{12}{(9-4r^2)\pi} & \frac{12(-1)^{r+1}}{(9-4r^2)\pi} \end{array} \right]^T & r \neq 0 \end{cases}. \quad (\text{A.51})$$

## 11 References

- 12 [1] A.S. Herrmann, P.C. Zahlen, I. Zuardy, Sandwich structures technology in commercial  
13      aviation, in: Proceedings of the 7th International Conference on Sandwich Structures,  
14      Aalborg, Denmark, August 2005, pp.13–26.
- 15 [2] H. Ning, G.M. Janowski, U.K. Vaidya, G. Husman, Thermoplastic sandwich structure  
16      design and manufacturing for the body panel of mass transit vehicle, *Compos. Struct.*  
17      80 (2007) 82–91.
- 18 [3] A. Mouritz, E. Gellert, P. Burchill, K. Challis, Review of advanced composite  
19      structures for naval ships and submarines, *Compos. Struct.* 53 (2001) 21–42.
- 20 [4] J. Hegger, M. Horstmann, Light-weight TRC sandwich building envelopes, in:

- 1        Proceedings of the Excellence in Concrete Construction through Innovation  
2        Conference, London, September 2008, pp.187–194.
- 3 [5] A. Ferreira, C. Roque, R. Jorge, E. Kansa, Static deformations and vibration analysis  
4        of composite and sandwich plates using a layerwise theory and multiquadratics  
5        discretizations, *Eng. Anal. Bound. Elem* 29 (2005) 1104–1114.
- 6 [6] N. Grover, D. Maiti, B. Singh, A new inverse hyperbolic shear deformation theory for  
7        static and buckling analysis of laminated composite and sandwich plates, *Compos.*  
8        *Struct.* 95 (2013) 667–675.
- 9 [7] E. Carrera, Historical reviews of zig-zag theories for multilayered plates and shells,  
10      *Appl. Mech. Rev.* 56 (2003) 287–308.
- 11 [8] M. Hajianmaleki, M.S. Qatu, Vibrations of straight and curved composite beams: a  
12      review, *Compos. Struct.* 100 (2013) 218–232.
- 13 [9] M. Kirugulige, R. Kitey, H. Tippur, Dynamic fracture behavior of model sandwich  
14      structures with functionally graded core: a feasibility study, *Compos. Sci. Technol* 65  
15      (2005) 1052–1068.
- 16 [10] Z. Kazancı, Z. Mecitoğlu, Nonlinear dynamic behavior of simply supported  
17      laminated composite plates subjected to blast load, *J. Sound Vib.* 317 (2008) 883–  
18      897.
- 19 [11] T. Park, S. Lee, J. Seo, G. Voyatzis, Structural dynamic behavior of skew sandwich  
20      plates with laminated composite faces, *Compos. Part B-Eng.* 39 (2008) 316–326.
- 21 [12] A. Allahverdizadeh, M. Mahjoob, M. Maleki, N. Nasrollahzadeh, M. Naei, Structural  
22      modeling, vibration analysis and optimal viscoelastic layer characterization of  
23      adaptive sandwich beams with electrorheological fluid core, *Mech. Res. Commun* 51  
24      (2013) 15–22.
- 25 [13] M. Alipour, M. Shariyat, Analytical zigzag formulation with 3D elasticity corrections  
26      for bending and stress analysis of circular/annular composite sandwich plates with  
27      auxetic cores, *Compos. Struct.* 132 (2015) 175–197.
- 28 [14] A. Adessina, M. Hamdaoui, C. Xu, Damping properties of bi-dimensional sandwich  
29      structures with multi-layered frequency-dependent visco-elastic cores, *Compos.*  
30      *Struct.* 154 (2016) 334–343.
- 31 [15] D. Chen, S. Kitipornchai, J. Yang, Nonlinear free vibration of shear deformable  
32      sandwich beam with a functionally graded porous core, *Thin Wall. Struct.* 107 (2016)  
33      39–48.
- 34 [16] N. Chikh, A. Nour, S. Aguib, I. Tawfiq, Dynamic analysis of the non-linear behavior  
35      of a composite sandwich beam with a magnetorheological elastomer core, *Acta Mech.*  
36      *Solida Sin.* 29 (2016) 271–283.
- 37 [17] W. Li, F. Sun, P. Wang, H. Fan, D. Fang, A novel carbon fiber reinforced lattice truss  
38      sandwich cylinder: fabrication and experiments, *Compos. Part A-Appl. Sci. Manuf.*  
39      81 (2016) 313–322.
- 40 [18] S. Sikdar, S. Banerjee, Guided wave propagation in a honeycomb composite  
41      sandwich structure in presence of a high density core, *Ultrasonics* 71 (2016) 86–97.
- 42 [19] S.K. Bapanapalli, O.M. Martinez, C. Gogu, B.V. Sankar, R.T. Haftka, M.L. Blosser,

- 1 Analysis and design of corrugated core sandwich panels for thermal protection  
2 systems of space vehicles, in: The 47th AIAA/ASME/ASCE/AHS/ASC Structures,  
3 Structural Dynamics, and Materials Conference, Newport, Rhode Island, May 2006,  
4 pp.1–18.
- 5 [20] J. Munch-Andersen, Improving thermal insulation of concrete sandwich buildings,  
6 *Indoor Built Environ.* 18 (2009) 424–431.
- 7 [21] E.M. Kerwin, Damping of flexural waves by a constrained viscoelastic layer, *J.  
8 Acoust. Soc. Am.* 31 (1959) 952–962.
- 9 [22] T.L. Teng, N.K. Hu, Analysis of damping characteristics for viscoelastic laminated  
10 beams, *Comput. Methods Appl. Mech. Eng* 190 (2001) 3881–3892.
- 11 [23] A. Kumar, S. Panda, Design of a 1-3 viscoelastic composite layer for improved  
12 free/constrained layer passive damping treatment of structural vibration, *Compos.  
13 Part B-Eng.* 96 (2016) 204–214.
- 14 [24] M.D. Rao, Recent applications of viscoelastic damping for noise control in  
15 automobiles and commercial airplanes, *J. Sound Vib.* 262 (2003) 457–474.
- 16 [25] C.M. Roland, Naval applications of elastomers, *Rubber Chem. Technol.* 77 (2004)  
17 542–551.
- 18 [26] C.A. Gallimore, Passive viscoelastic constrained layer damping application for a  
19 small aircraft landing gear system, Master Thesis, Virginia Polytechnic Institute and  
20 State University, 2008.
- 21 [27] Q. Ni, Y. Xiang, Y. Huang, J. Lu, Modeling and dynamics analysis of shells of  
22 revolution by partially active constrained layer damping treatment, *Acta Mech.  
23 Solida Sin.* 26 (2013) 468–479.
- 24 [28] P. Datta, M. Ray, Three-dimensional fractional derivative model of smart constrained  
25 layer damping treatment for composite plates, *Compos. Struct.* 156 (2015) 291–306.
- 26 [29] V. Narayananamurti, H. Störmer, M. Chin, A. Gossard, W. Wiegmann, Selective  
27 transmission of high-frequency phonons by a superlattice: The "dielectric" phonon  
28 filter, *Phys. Rev. Lett.* 43 (1979) 2012–2016.
- 29 [30] Z. Liu, X. Zhang, Y. Mao, Y. Zhu, Z. Yang, C. Chan, P. Sheng, Locally resonant  
30 sonic materials, *Science* 289 (2000) 1734–1736.
- 31 [31] M.I. Hussein, M.J. Leamy, M. Ruzzene, Dynamics of phononic materials and  
32 structures: Historical origins, recent progress, and future outlook, *Appl. Mech. Rev.*  
33 66 (2014) 040802.
- 34 [32] D.R. Smith, J.B. Pendry, M.C. Wiltshire, Metamaterials and negative refractive index,  
35 *Science* 305 (2004) 788–792.
- 36 [33] D. Del Vescovo, I. Giorgio, Dynamic problems for metamaterials: review of existing  
37 models and ideas for further research, *Int. J. Eng. Sci.* 80 (2014) 153–172.
- 38 [34] P.A. Deymier, *Acoustic metamaterials and phononic crystals*, Springer Science &  
39 Business Media, New York, 2013.
- 40 [35] M. Ruzzene, F. Scarpa, Control of wave propagation in sandwich beams with auxetic  
41 core, *J. Intell. Mater. Syst. Struct.* 14 (2003) 443–453.
- 42 [36] J. Wen, X. Wen, D. Yu, Flexural vibration band gaps in periodic sandwich beams

- 1 with auxetic core, in: ASME 2007 International Design Engineering Technical  
2 Conferences & Computers and Information in Engineering Conference, Las Vegas,  
3 USA, September 2007, pp.1–5.
- 4 [37] H. Badran, M. Tawfik, H. Negm, Vibration characteristics of periodic sandwich  
5 beams, in: 13th International Conference on Applied Mechanics and Mechanical  
6 Engineering, Cairo, Egypt, May 2008, pp.1–15.
- 7 [38] J.S. Chen, S.M. Tsai, Sandwich structures with periodic assemblies on elastic  
8 foundation under moving loads, *J. Vib. Control* 22 (2016) 2519–2529.
- 9 [39] P. Wei, Y. Zhao, The influence of viscosity on band gaps of 2D phononic crystal,  
10 *Mech. Adv. Mater. Struct.* 17 (2010) 383–392.
- 11 [40] R.P. Moiseyenko, V. Laude, Material loss influence on the complex band structure  
12 and group velocity in phononic crystals, *Phys. Rev. B* 83 (2011) 064301.
- 13 [41] J.H. Oh, Y.J. Kim, Y.Y. Kim, Wave attenuation and dissipation mechanisms in  
14 viscoelastic phononic crystals, *J. Appl. Phys* 113 (2013) 106101.
- 15 [42] Y. Wang, Y. Wang, V. Laude, Wave propagation in two-dimensional viscoelastic  
16 metamaterials, *Phys. Rev. B* 92 (2015) 104110.
- 17 [43] Z. Guo, M. Sheng, J. Pan, Flexural wave attenuation in a sandwich beam with  
18 viscoelastic periodic cores, *J. Sound Vib.* 400 (2017) 227–247.
- 19 [44] W.L. Li, X. Zhang, J. Du, Z. Liu, An exact series solution for the transverse vibration  
20 of rectangular plates with general elastic boundary supports, *J. Sound Vib.* 321 (2009)  
21 254–269.
- 22 [45] L. Brillouin, *Wave Propagation in Periodic Structures*, Dover Publication, New York:  
23 Dover, 1953.
- 24

25 **Figure Captions:**

- 26 **Fig. 1** Schematic diagram of an infinite sandwich plate with viscoelastic periodic cores.
- 27 **Fig. 2.** Coordinates and notations of a sandwich plate.
- 28 **Fig. 3.** Denotations of generalized forces in a sandwich plate.
- 29 **Fig. 4.** A finite periodic sandwich plate.
- 30 **Fig. 5.** Boundary conditions in a finite periodic sandwich plate.
- 31 **Fig. 6.** A unit element with periodic boundary condition.
- 32 **Fig. 7.** Band structure in an infinite periodic sandwich plate. (BG: Band gap.)
- 33 **Fig. 8.** Averaged velocity response of the last sub sandwich plate in a finite periodic  
34 sandwich plate. (BG: Band gap.)
- 35 **Fig. 9.** (a) Overall dispersion branches and dispersion branches in the (b) first, (c) second,  
36 (d) third, (e) fourth, and (f) fifth cross-stream modal groups. (BG: band gap; the  
37 letters from ‘a’ to ‘k’ beside the circle ‘○’ denote the sub figure indices of

1           **Fig. 10.)**

2       **Fig. 10.** Displacement amplitude distribution of a unit element at  $q_n = 0.75$  for the  
3       dispersion branches in the first ((a) 1<sup>#1</sup>, (b) 1<sup>#2</sup>, and (c) 1<sup>#3</sup>), second ((d) 2<sup>#1</sup>, (e) 2<sup>#2</sup>,  
4       and (f) 2<sup>#3</sup>), third ((g) 3<sup>#1</sup> and (h) 3<sup>#2</sup>), fourth ((i) 4<sup>#1</sup> and (j) 4<sup>#2</sup>), and fifth ((k) 5<sup>#1</sup>)  
5       cross-stream modal groups.

6       **Fig. 11.** Effects of dimensional parameters of (a) element length, (b) length ratio, (c)  
7       element width, and (d) core thickness on band-gap frequency and band-gap width.

8       **Fig. 12.** Effects of (a) Young's modulus of soft core  $E_A$  and (b) Young's modulus of hard  
9       core  $E_B$  on band-gap frequency and band-gap width.

10      **Fig. 13.** Effect of damping on averaged velocity response of the last sub sandwich plate.

11      **Fig. 14.** Damping effect of independent soft core (core A) and independent hard core  
12       (core B) on vibration response with (a) comparison between case 1 and case 2 and  
13       (b) comparison between case 3 and case 4.

14      **Fig. 15.** Comparisons of averaged velocity response of the last sub sandwich plate among  
15       three sandwich plates with (a) comparison between periodic cores and uniform  
16       soft core and (b) comparison between periodic cores and uniform hard core.

17      **Fig. 16.** Periodic cores of the tested sandwich plate.

18      **Fig. 17.** Schematic diagram of experimental set-up.

19      **Fig. 18.** Practical experimental set-up.

20      **Fig. 19.** Comparison of average responses between the left-end region and right-end  
21       region in the sandwich specimen. (BG: band gap.)

22      **Fig. 20.** Band structure calculated by present analytical model. (BG: band gap.)

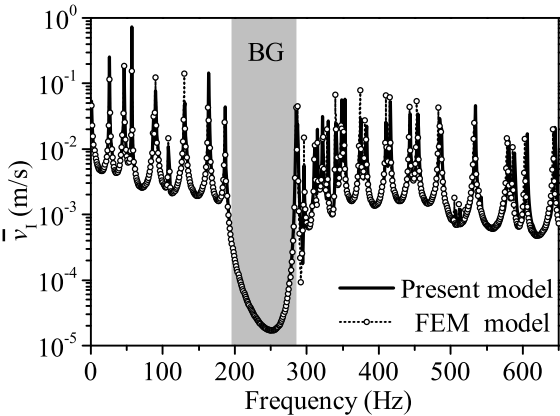
23

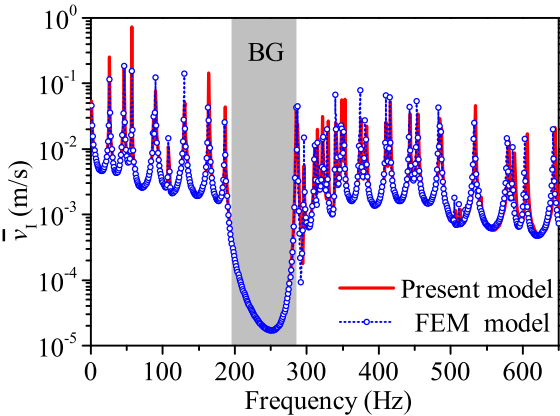
24      **Table Captions:**

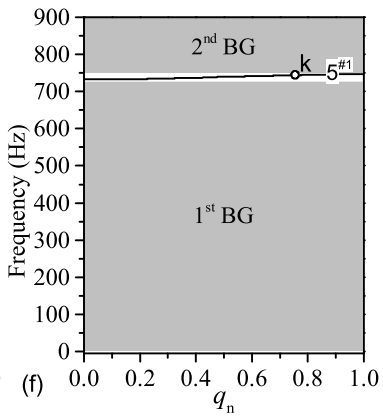
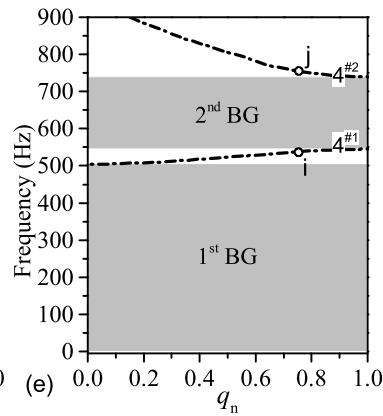
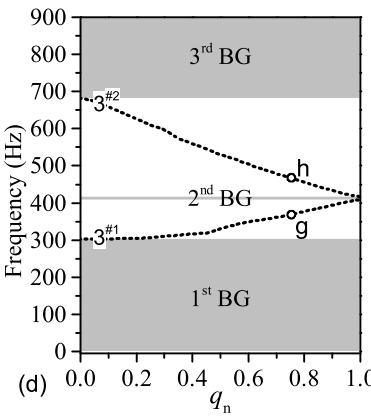
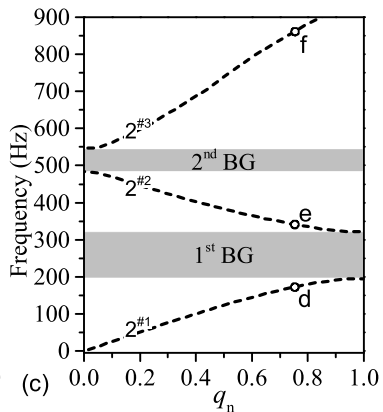
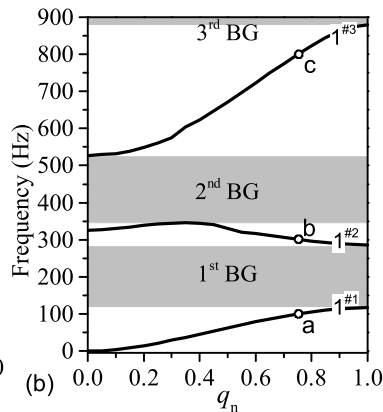
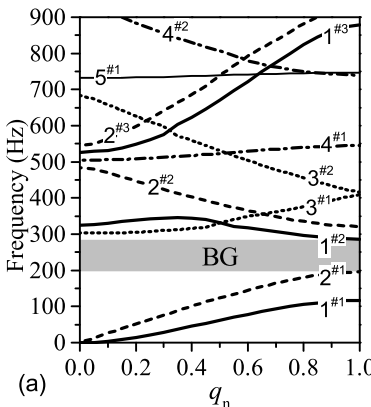
25      **Table 1** Dimensions and material parameters of a unit element.

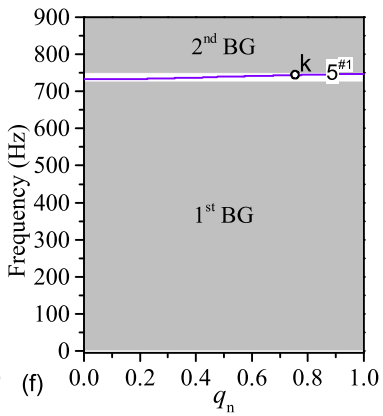
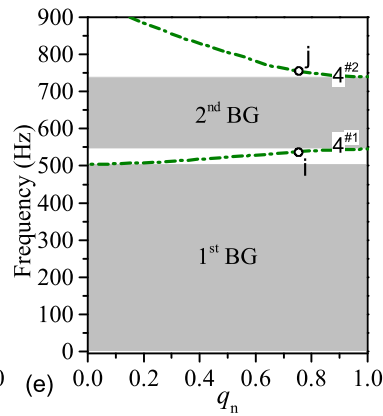
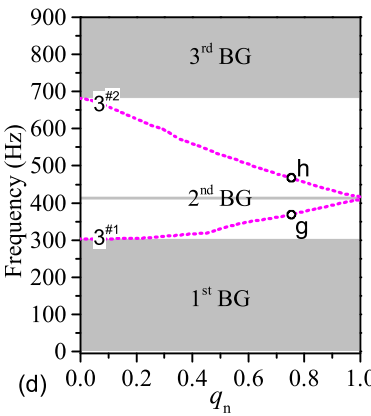
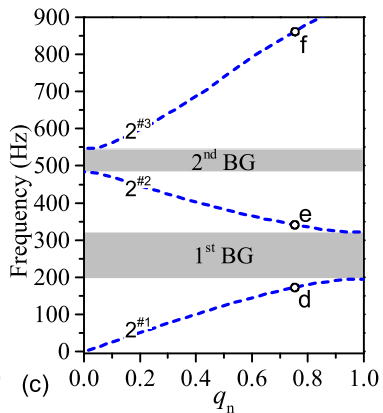
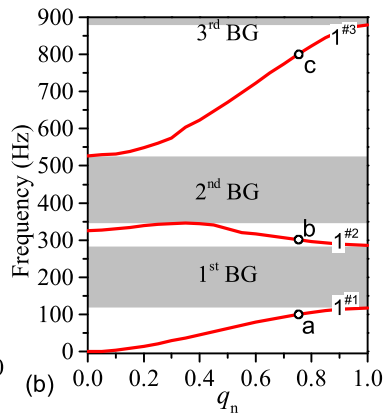
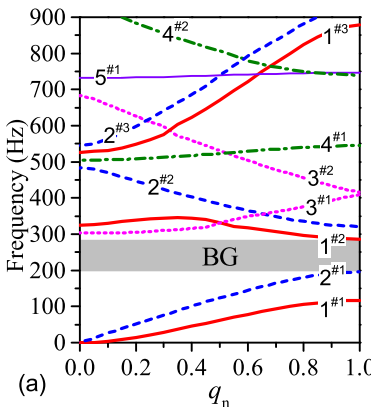
26      **Table 2** Overall band gap and cross-stream modal band gaps of a periodic sandwich plate.

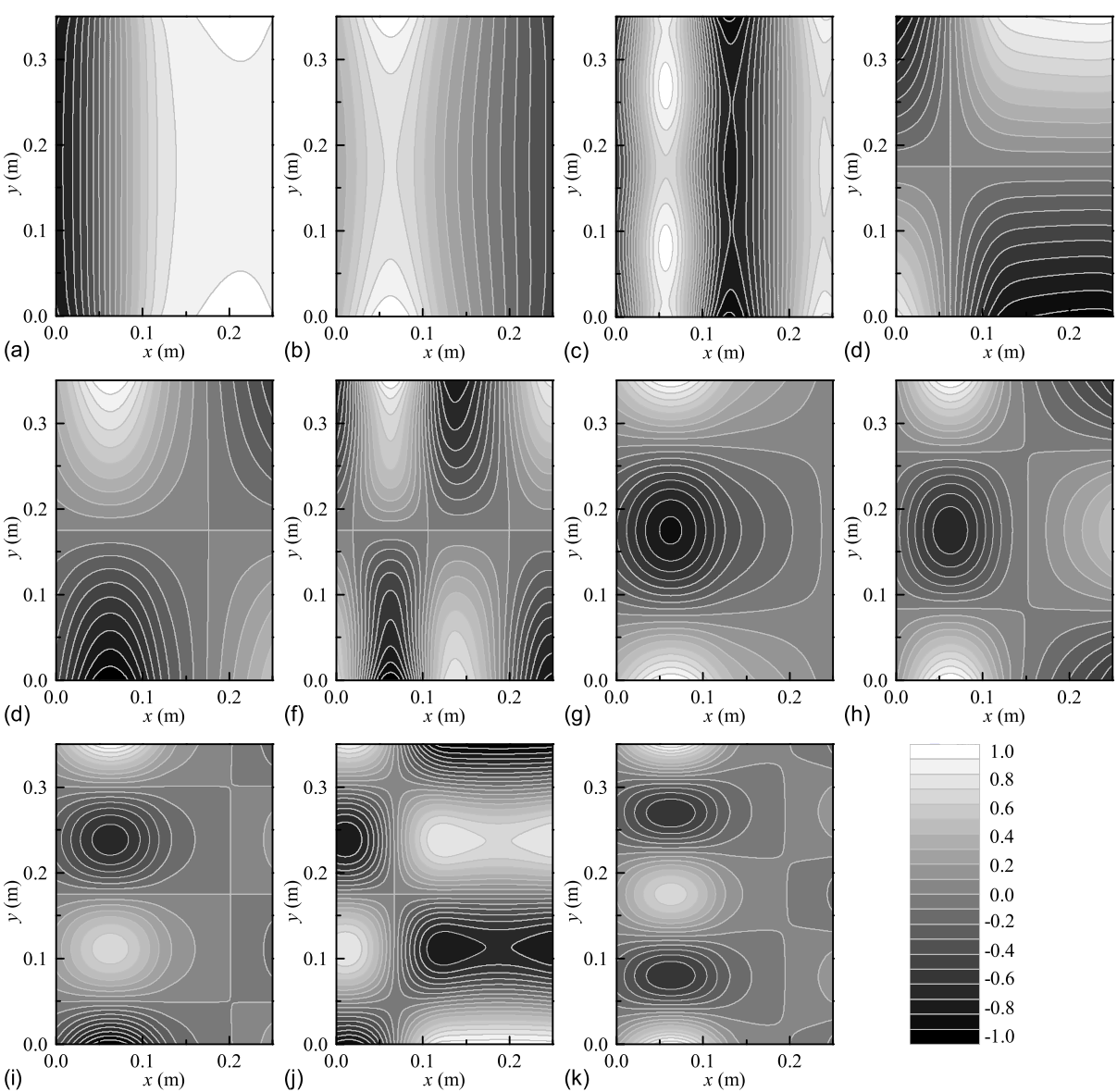
27

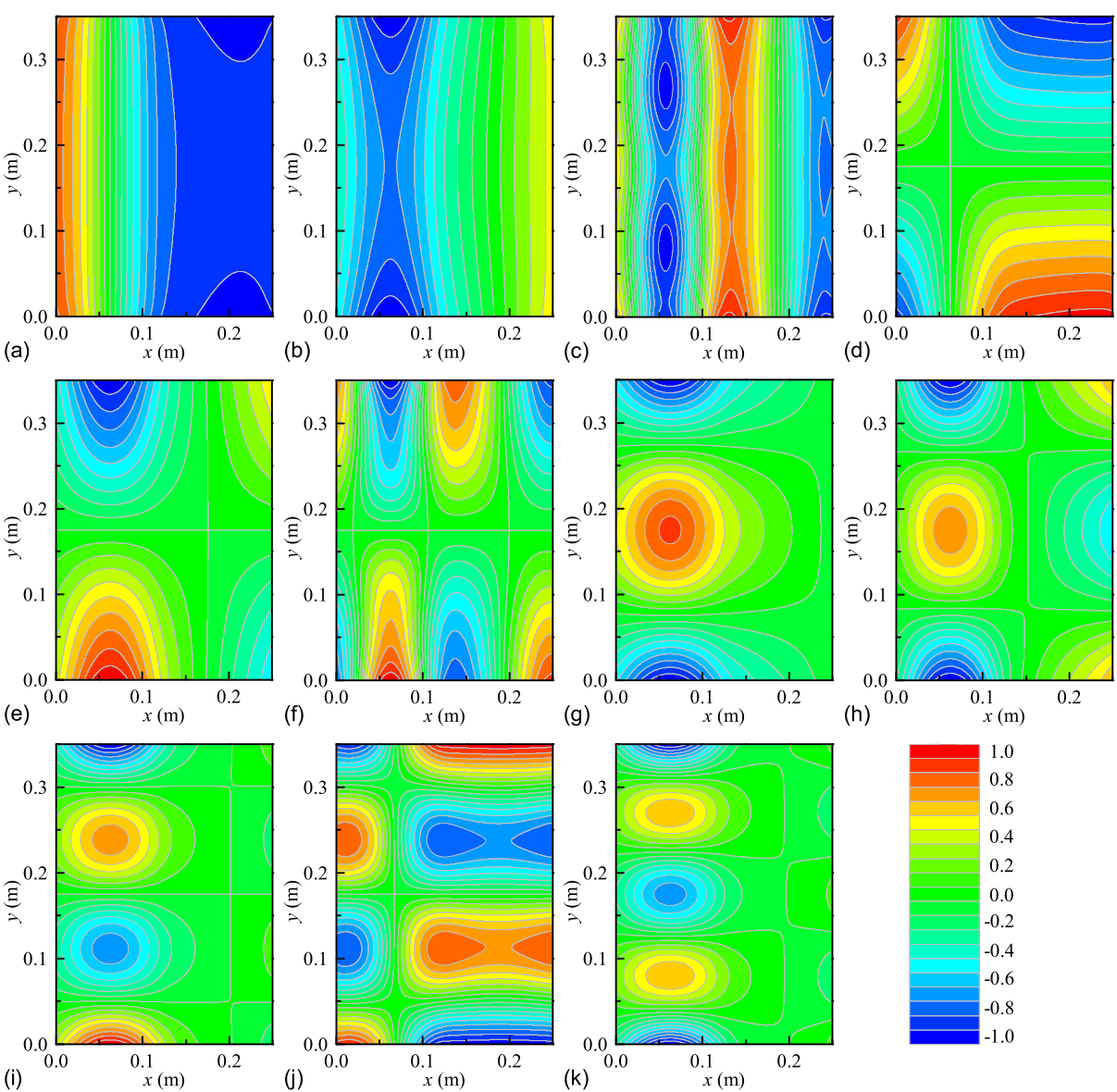


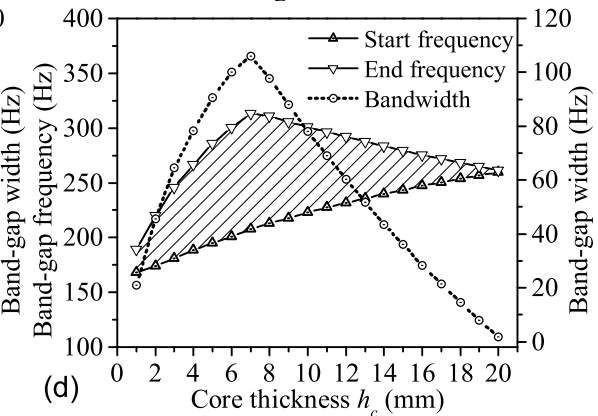
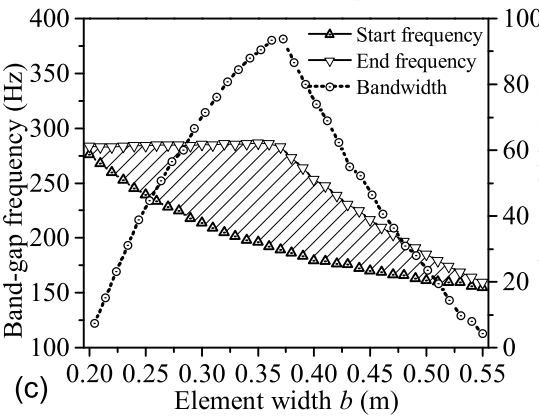
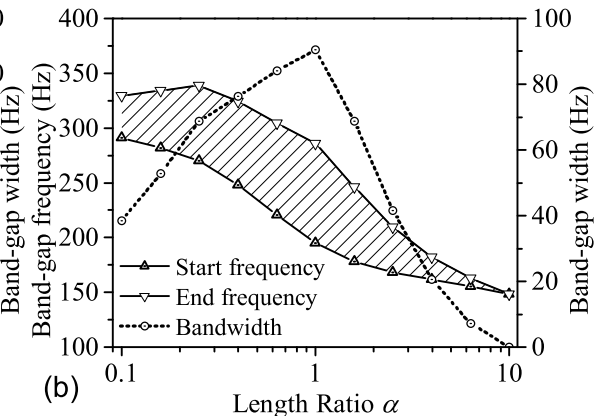
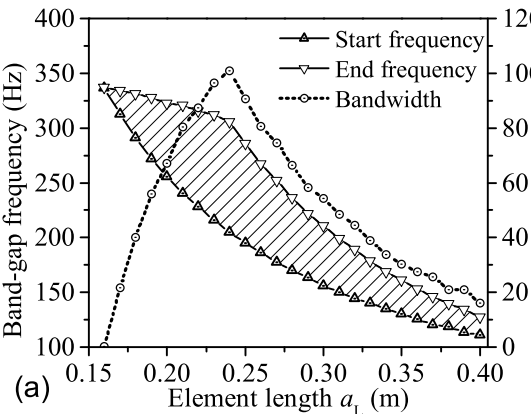


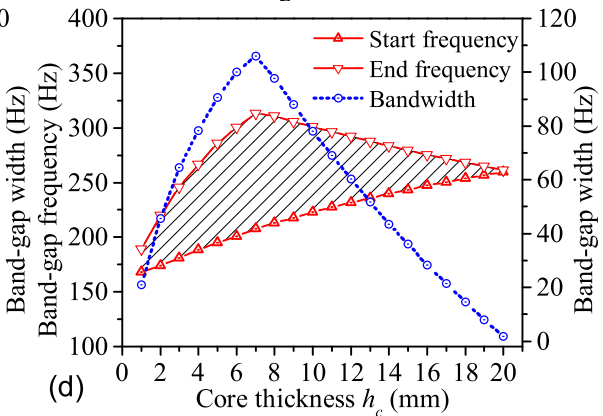
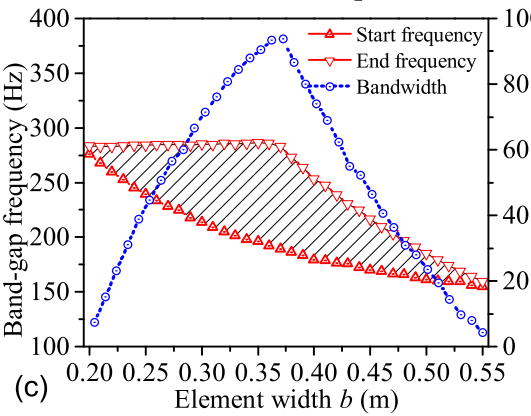
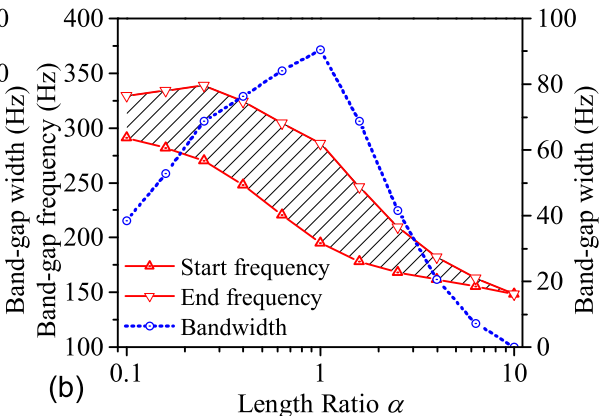
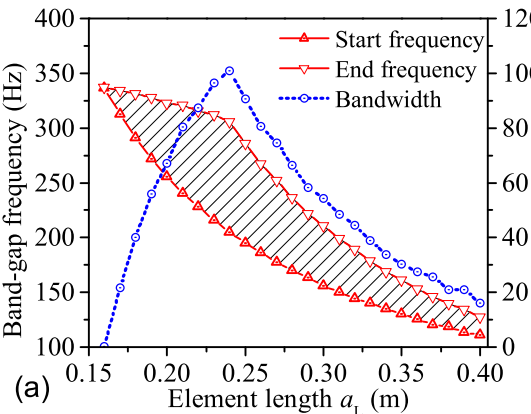


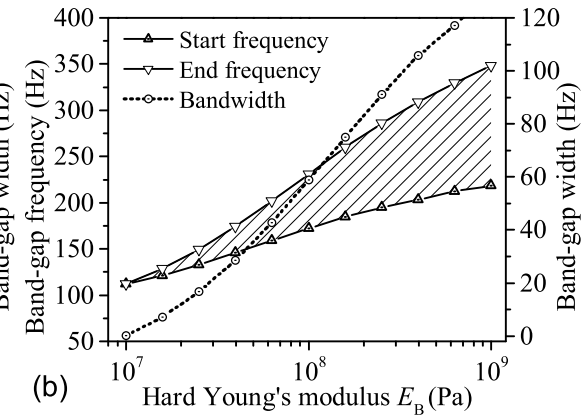
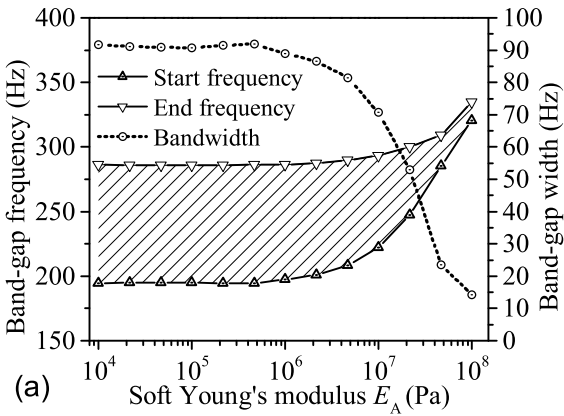


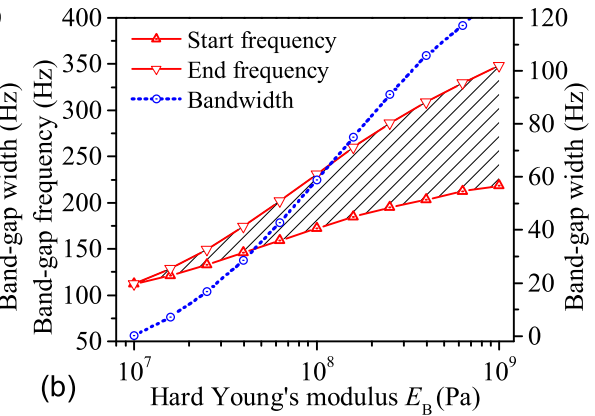
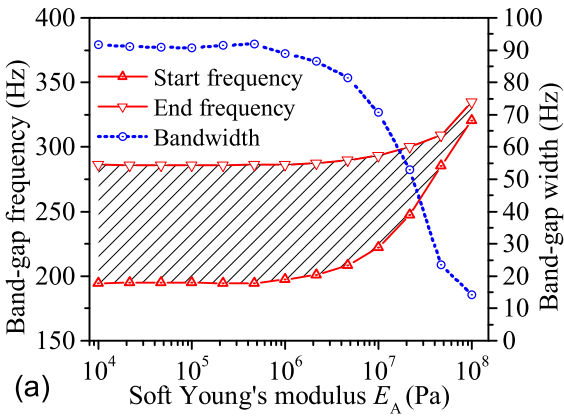


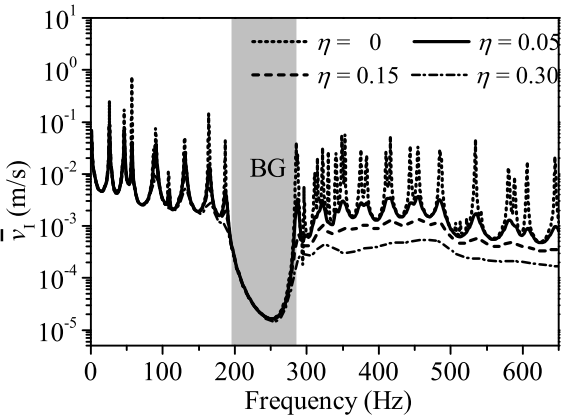


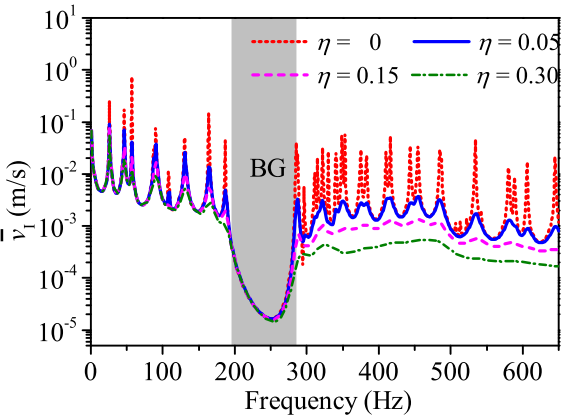


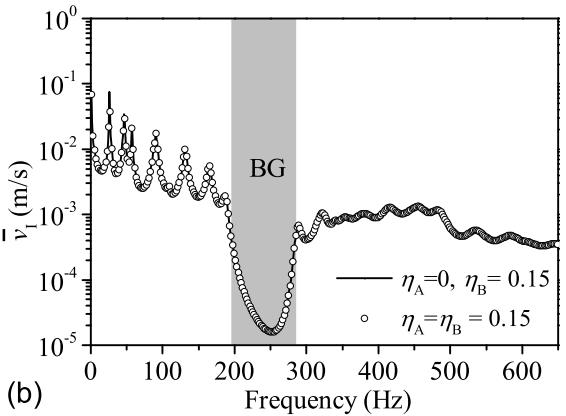
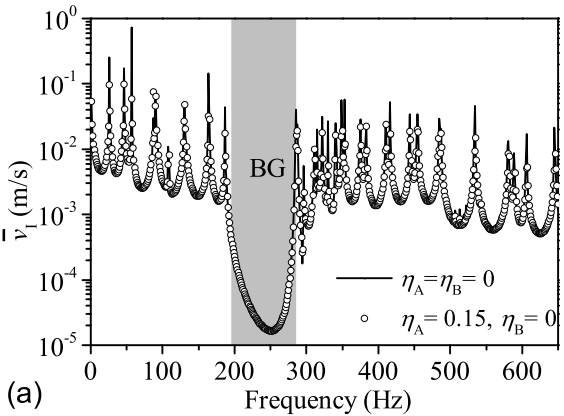


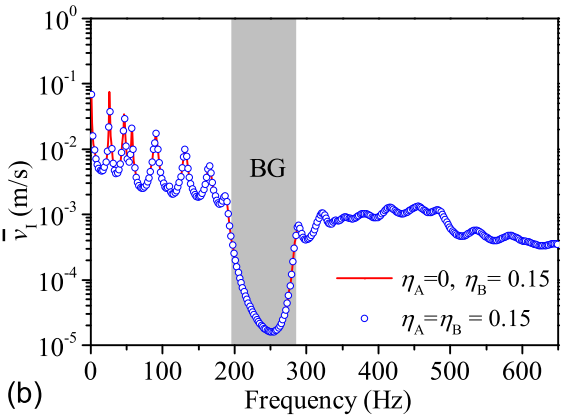
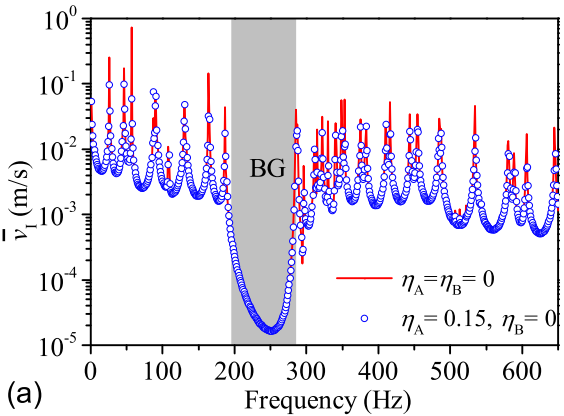


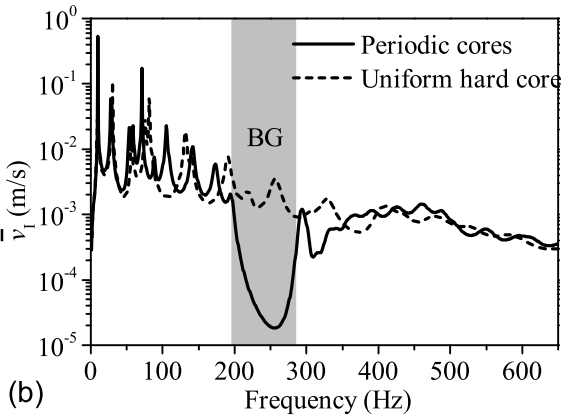
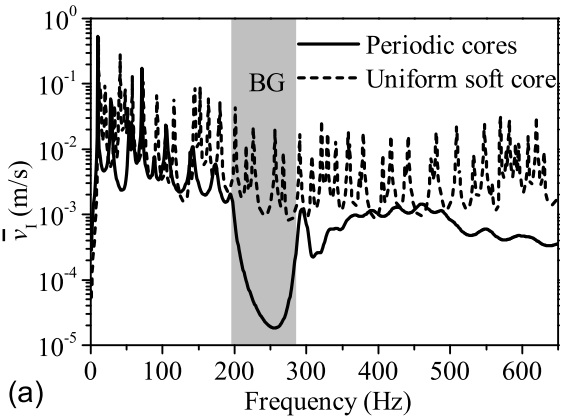


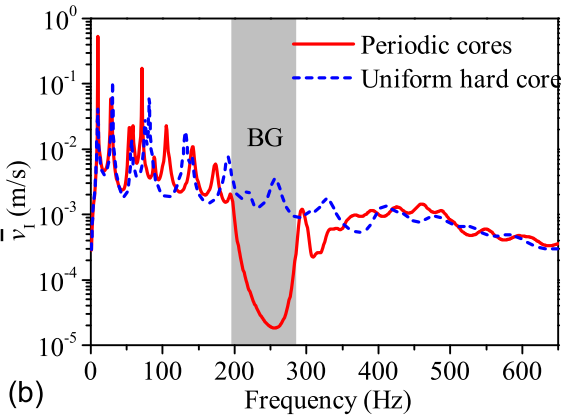
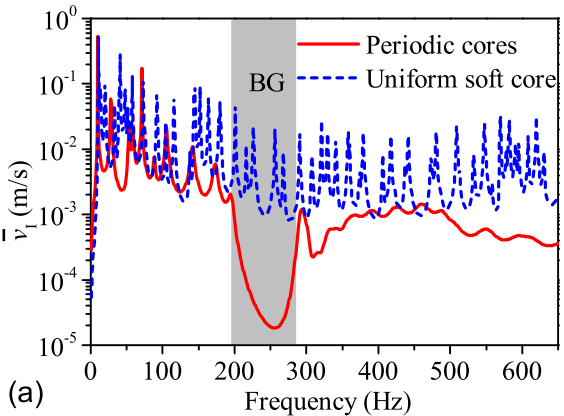






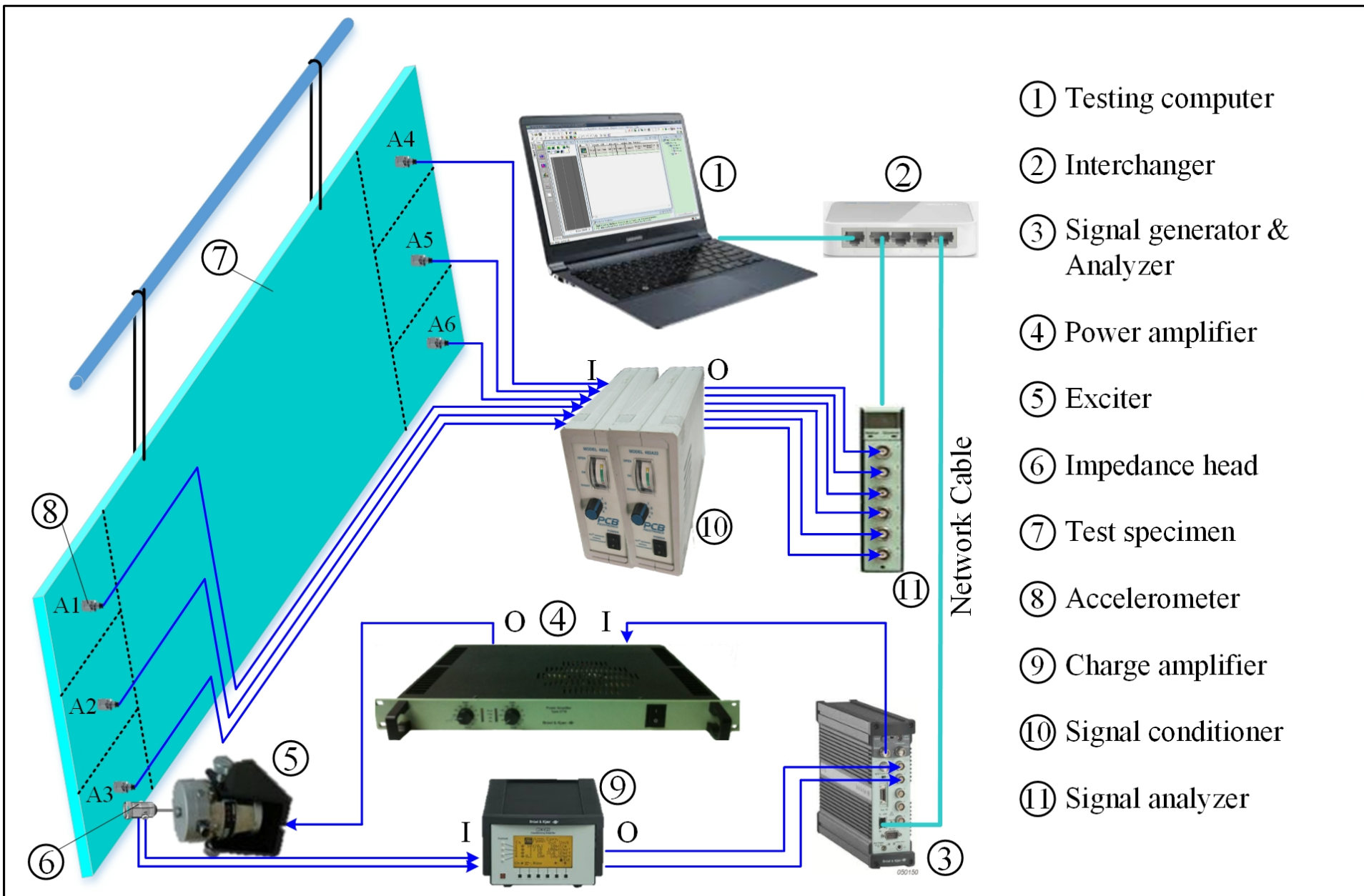


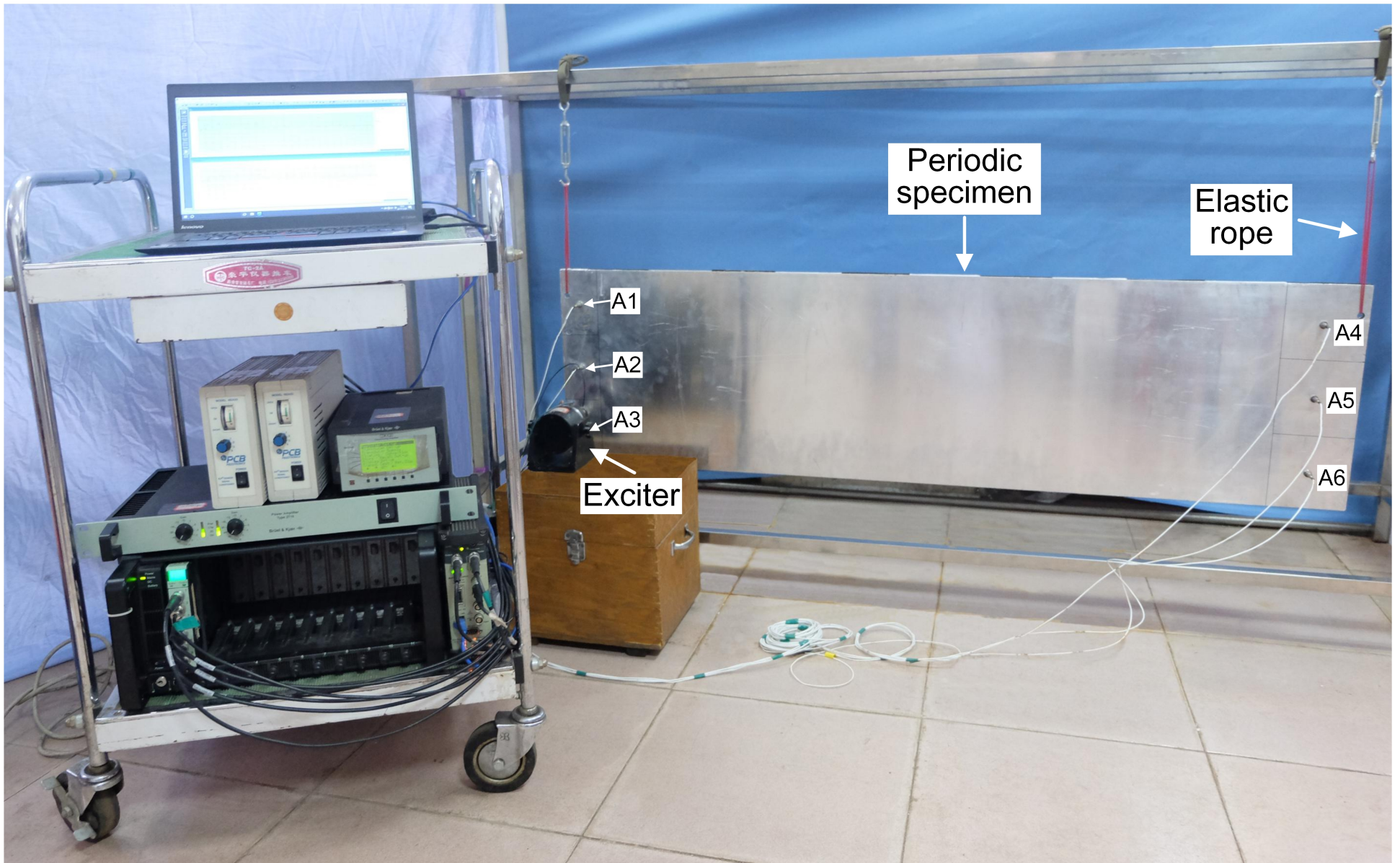


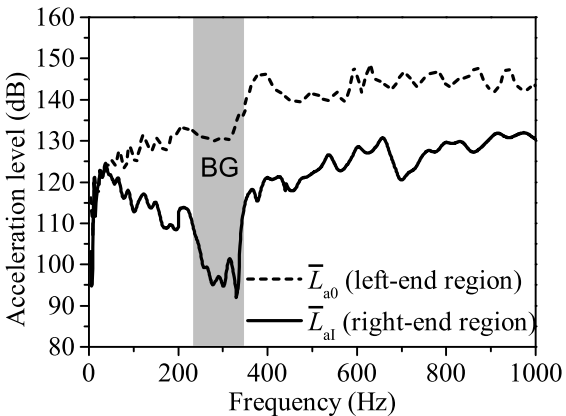


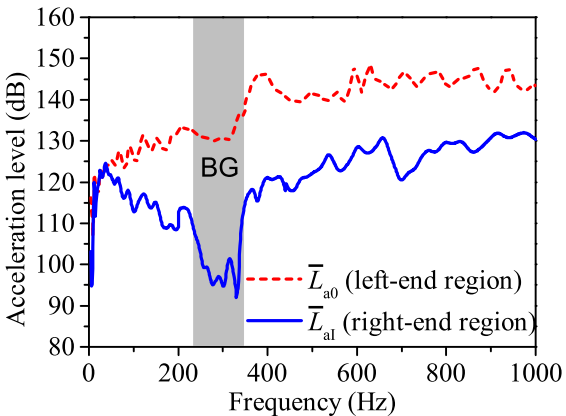


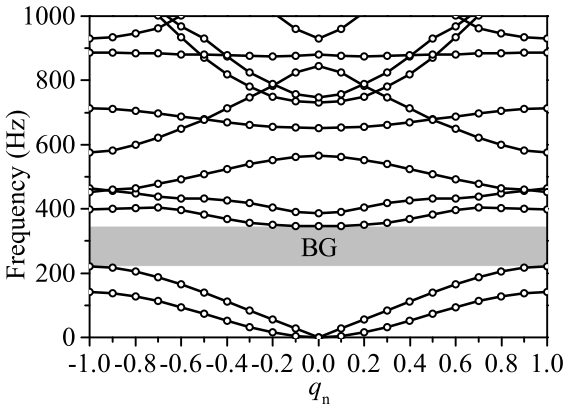


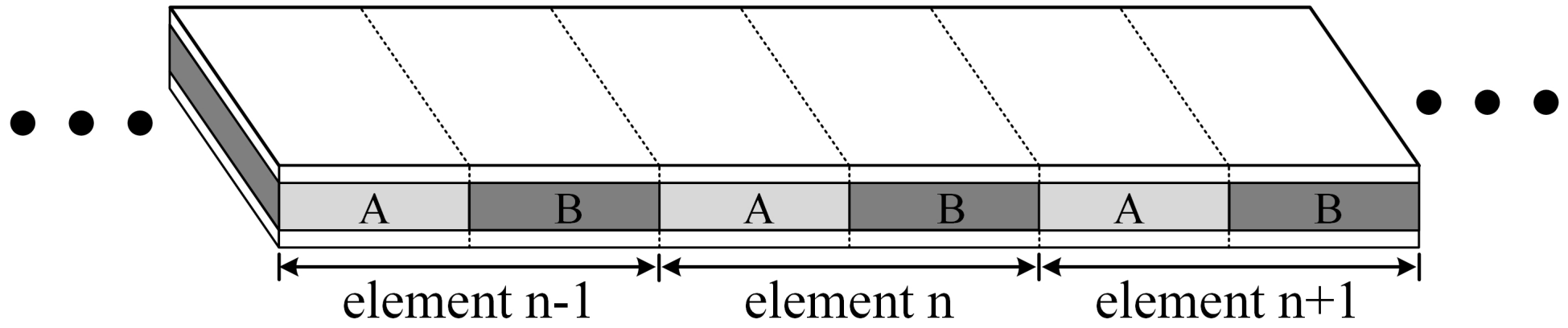


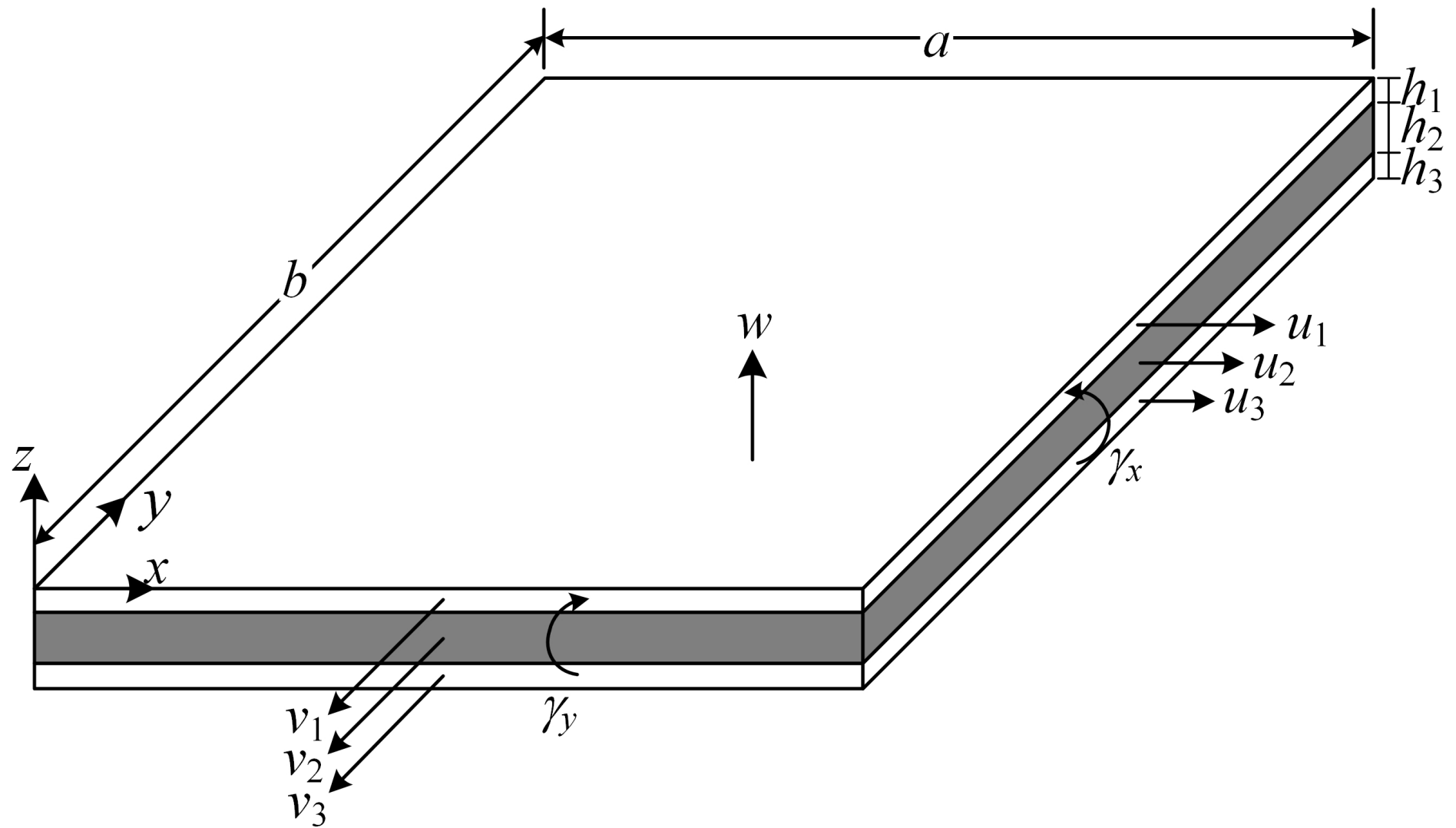


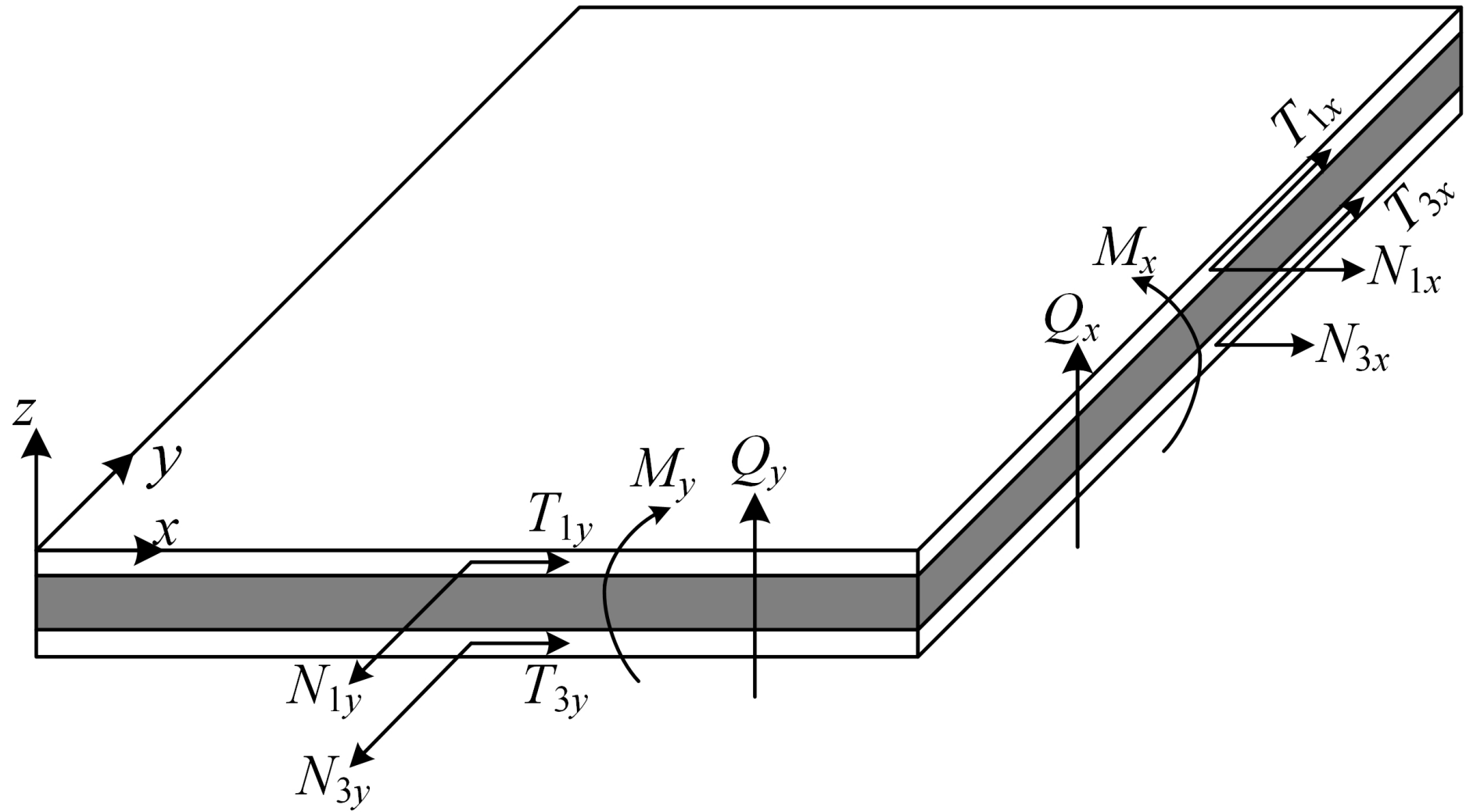


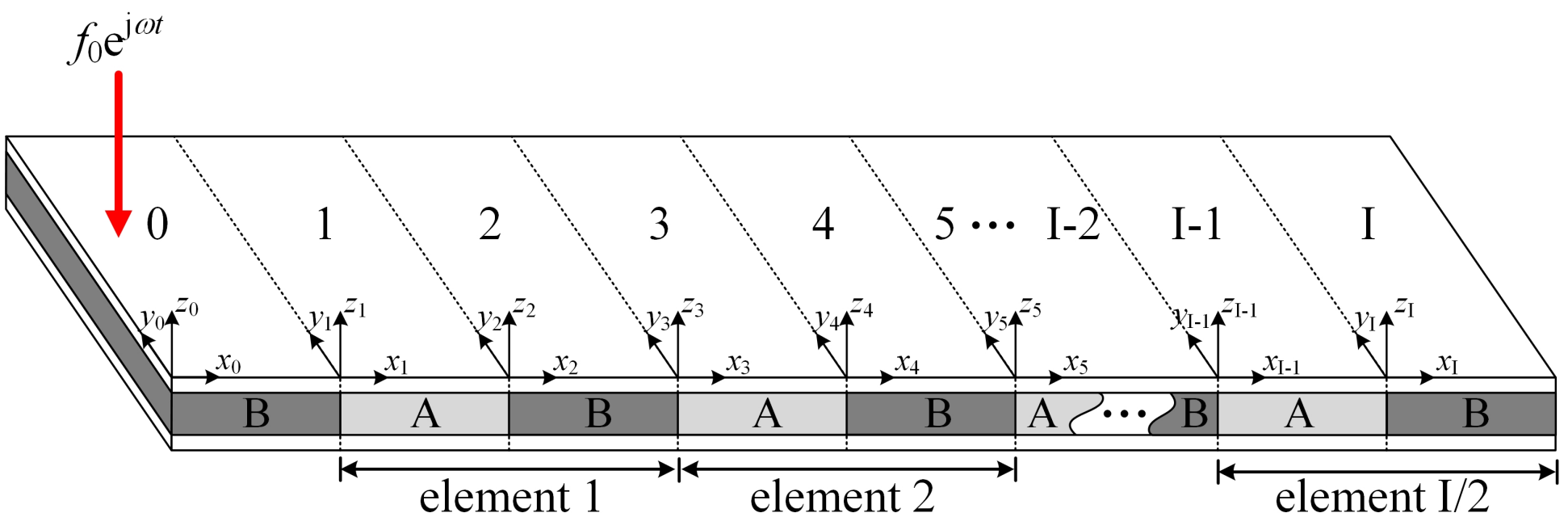


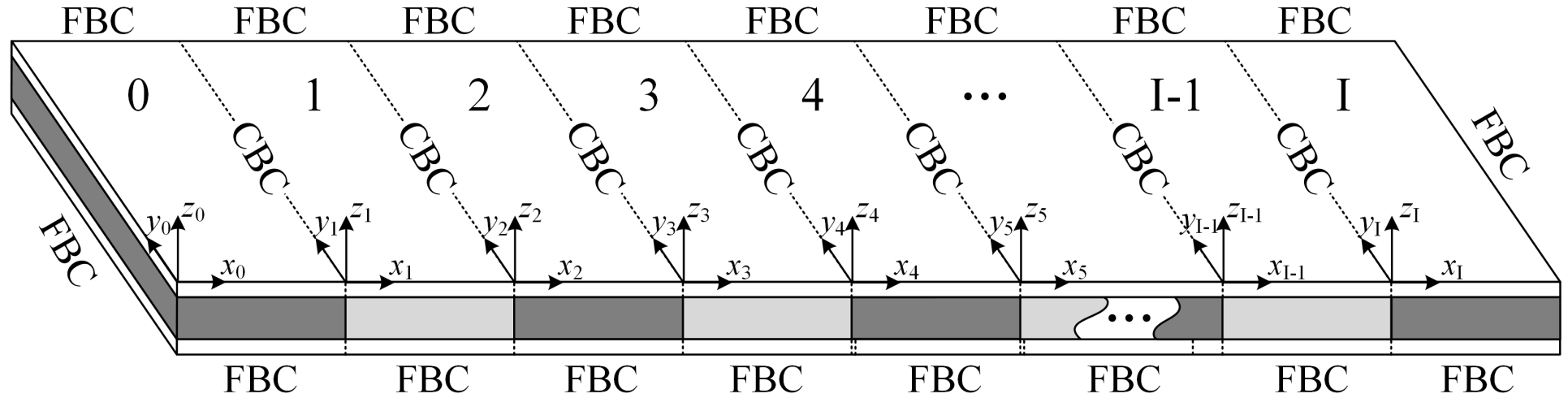


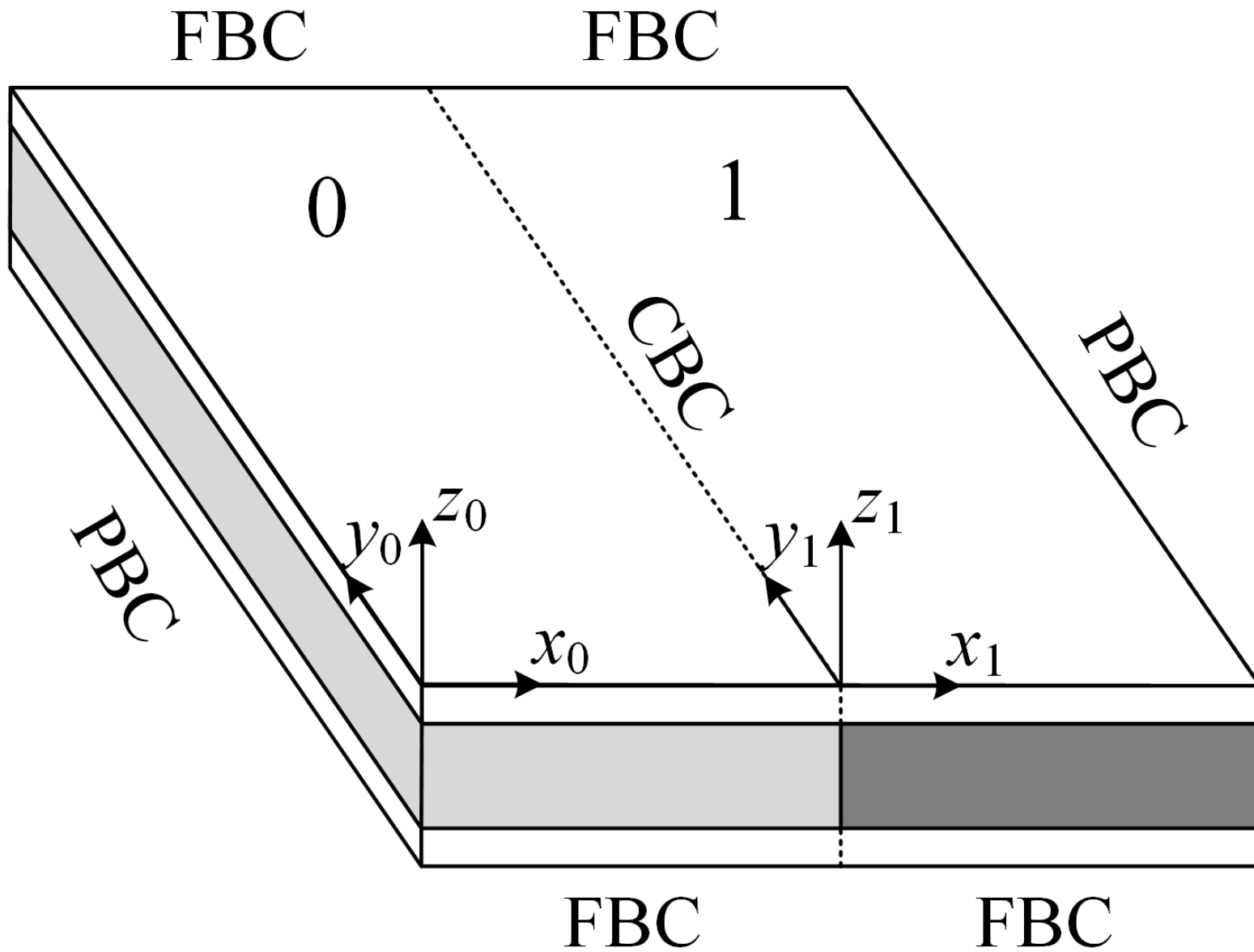


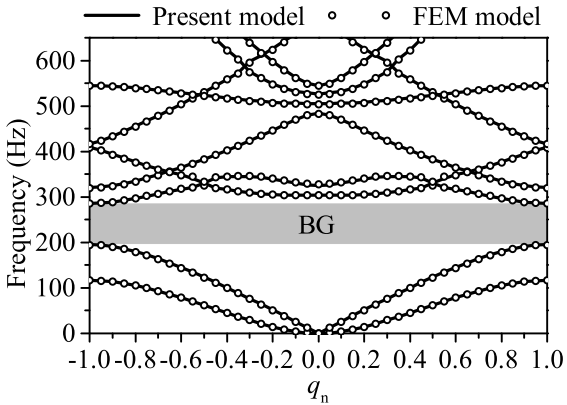












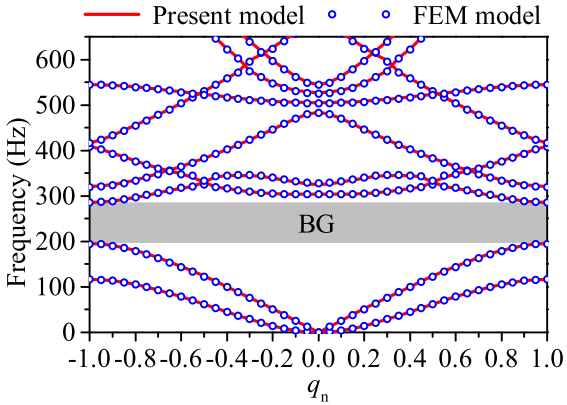


**Table 1** Dimensions and material parameters of a unit element.

	$E_s$ (GPa)	$G_s$ (GPa)	$\rho$ (kg·m <sup>-3</sup> )	$\nu$	$a$ (m)	$b$ (m)	$h$ (mm)
Bottom layer	77.6	28.7	2730	0.35	0.250	0.35	2.0
Core A	$1.38 \times 10^{-4}$	$5.11 \times 10^{-5}$	332	0.35	0.125	0.35	5.0
Core B	$2.50 \times 10^{-1}$	$8.39 \times 10^{-2}$	1100	0.49	0.125	0.35	5.0
Top layer	77.6	28.7	2730	0.35	0.250	0.35	1.8

**Table 1** Overall band gap and cross-stream modal band gaps of a periodic sandwich plate.

	1 <sup>st</sup> modal group	2 <sup>nd</sup> modal group	3 <sup>rd</sup> modal group	4 <sup>th</sup> modal group	5 <sup>th</sup> modal group	Overall
1 <sup>st</sup> BG (Hz)	116.8–286.0	195.3–321.3	0–303.8	0–504.5	0–732.4	195.3–286.0
2 <sup>nd</sup> BG (Hz)	344.8–526.6	479.4–544.9	409.5–417.1	545.0–739.8	746.5–900	N/A
3 <sup>rd</sup> BG (Hz)	878.6–900	N/A	682.2–900	N/A	N/A	N/A